交通大學聯發科研究中心子計畫
所屬分項之技術報告

用於正交分頻多工數位視訊廣播系統之
接收多樣與相位雜訊補償技術

Diversity Reception and Phase Noise Compensation in OFDM-Based DVB Systems

計畫主持人： 李大嵩 教授
計畫參與人員： 紀宜志、楊松根

執行單位：國立交通大學電信工程系

執行期間：九十二年八月一日至九十三年七月三十一日

用於正交分頻多工數位視訊廣播系統之接收多樣與相位雜訊補償技術

學生：紀宜志　　指導教授：李大嵩 博士

國立交通大學電信工程學系碩士班

摘要

正交分頻多工為一種具高頻譜效益，並能有效地克服多路徑衰落效應的調變技術。使用正交分頻多工技巧之數位視訊廣播(OFDM-based DVB)系統，具有對抗碼際干擾之強韌性及高頻譜效益，這些利基驅使研發單位與產業界競相投入該種系統之設計與實現。在本論文中，吾人提出一種具有接收多樣與相位雜訊補償能力之 OFDM-based DVB 接收機，能有效對抗多路徑衰落及相位擾動現象。一般而言，行動通訊系統受到多路徑干擾之時變性衰落通道的影響，易造成系統效能大幅降低，吾人將針對此問題對接收機之各個層級提出接收多樣方法，藉以減緩時變性衰落效應。另一方面，為了能夠充分地改善空時頻無線通道之相位雜訊問題，吾人針對相位雜訊補償，提出「空時頻回授決策法」，利用相鄰載波通道間高相關之特性，選擇最佳資料取樣大小，並將資料以最小平均平方誤差法則計算相對應之載波加權值，以取代原本的通道估測。此種批次處理法可在載波通道變化及相位雜訊補償上取得一平衡點。最後，吾人藉由電腦模擬驗證上述架構在市區無線環境中，具有優異的傳輸表現。

Diversity Reception and Phase Noise Compensation in OFDM-Based DVB Systems

Student: Ji-Chi Chi Advisor: Dr. Ta-Sung Lee

Institute of Communication Engineering

National Chiao Tung University

Abstract

Orthogonal frequency division multiplexing (OFDM) is a high spectral efficiency modulation technique that can successfully alleviate multipath fading effects. Digital video broadcasting (DVB) systems incorporating the OFDM technique, which can promise robustness against intersymbol interference (ISI) and efficiency in spectrum utilization, are attracting researchers and industry attention to its design and implementation. In this thesis, an OFDM-based DVB receiver with diversity reception and phase noise compensation schemes is proposed, which provides diversity gain and phase noise suppression simultaneously. Performance of a mobile communication system is typically significantly degraded due to time-varying fading channels. To mitigate this problem, diversity reception schemes at different stages of the receiver are designed to alleviate the fading effects. On the other hand, to alleviate the phase noise effect over space-time-frequency wireless channels, we propose a space-time-frequency decision feedback algorithm for phase noise compensation, in which the optimum data sample size is selected based on the high correlation between adjacent data tones. Batches of the data samples are then processed with the minimum mean square error (MMSE) criterion to obtain the optimum weights at the corresponding data tones. The batch processing can achieve a good balance between channel variation and phase noise compensation. Finally, we evaluate the performance of the proposed system and confirm that it works well in a typical urban environment.

Acknowledgement

I would like to express my deepest gratitude to my advisor, Dr. Ta-Sung Lee, for his enthusiastic guidance and great patience. I learn a lot from his positive attitude in many areas. Heartfelt thanks are also offered to all members in the Communication Signal Processing (CSP) Lab for their constant encouragement. Finally, I would like to show my sincere thanks to my parents and Nall for their invaluable love and love.

Contents

List of Figures

List of Tables

Acronym Glossary

ACS	add-compare-select
BCH	Bose-Chaudhuri-Hocquenghem
BER	bit error rate
COFDM	coded orthogonal frequency division multiplexing
CDD	cyclic delay diversity
CPE	common phase error
DD	delay diversity
DFT	discrete Fourier transform
DTV	digital television
DVB	digital video broadcasting
DVB-H	DVB-handheld
DVB-T	DVB-terrestrial
ETSI	European Telecommunication Standard Institute
FFT	fast Fourier transform
FIFO	first-input first-output
ICI	intercarrier interference
IDFT	inverse DFT
IEEE	institute of electrical and electronics engineers
IFFT	inverse fast Fourier transforms
ISI	intersymbol interference
IVSD	in-Viterbi selective diversity
LS	least square
MMSE	minimum mean square error
MRC	maximal ratio combining
OFDM	orthogonal frequency division multiplexing
PBSD	packet-based selective diversity

PD	phase diversity
PRBS	pseudo random binary sequence
PVSD	post-Viterbi selective diversity
QAM	quadrature amplitude modulation
QPSK	quaternary phase shift keying
RF	radio frequency
RS	Reed-Solomon
RX	receiver
SBSD	symbol-based selective diversity
SFN	single frequency network
SNR	signal-to-noise ratio
TPS	transmission parameter signaling

Notations

B	system bandwidth
B_c	coherence bandwidth
f_d	Doppler frequency
E_b	bit energy
E_s	symbol energy
$h^{(l)}$	channel gain from the transmit antenna to the *l*th receive antenna
N_c	number of subcarriers (FFT/IFFT size)
N_{cp}	number of guard interval samples
N_r	number of receive antenna
T_c	coherence time
T_s	symbol duration
T_{sample}	sampling period
v	mobile velocity
$\mathbf{w}_d$	weighting vector on the data tone for phase noise compensation
N_b	sample size
$N_k^{(1)}(n)$	additive white noise at the *k*th data tone, *l*th antenna and *n*th OFDM symbol
$Y_k^{(1)}(n)$	received data at the *k*th data tone, *l*th antenna and *n*th OFDM symbol
$X_k^{(1)}(n)$	transmitted data at the *k*th data tone, *l*th antenna and *n*th OFDM symbol
σ^2	noise power
γ	instantaneous SNR
τ_{rms}	root mean squared excess delay spread
ϕ	phase noise

Chapter 1

Introduction

With the fast development of personal communications and increasing need of multi-media messaging, digital video broadcasting (DVB) is now widely deployed around the world. However, the physical limitation of the wireless channel, typically subject to both time-selective and frequency-selective fading induced by phase noise, Doppler shift and multipath propagation, presents a fundamental challenge to reliable communications. As a remedy, several signal processing techniques shall be developed to alleviate the transmission distortions caused by wireless communication environments. Hence, recent research efforts are carried out to design diversity reception [1]-[7], and phase noise compensation schemes [8]-[22] with sophisticated signal processing algorithms to deliver a feasible solution for advanced digital television (DTV) and create a portfolio of corresponding intellectual properties.

DVB-terrestrial (DVB-T), which is probably the most complex DVB delivery system, has been standardized in February 1997 [23], and programs/services have started in several European countries a few years ago. The corresponding transmission scheme of DVB-T systems is based on the coded orthogonal frequency division multiplexing (COFDM) principle [24], whose origin goes back to the 1960s, and was considered recently for mobile radio services. COFDM is a multipath-friendly mechanism that treats the whole transmission band as a set of adjacent narrow sub-bands. This property leads OFDM to be chosen over a single-carrier solution to avoid using a complicated equalizer, which is usually a heavy burden in a wideband communication receiver. Moreover, with proper coding and interleaving across

frequencies, multipath turns into an OFDM system advantage by yielding frequency diversity. OFDM can be implemented efficiently by using the Fast Fourier Transform (FFT) at the transmitter and receiver. At the receiver, FFT reduces the channel response into a multiplicative constant on a tone-by-tone basis.

Diversity is a well-known approach to combating fading, and is also a very effective way to combat Doppler shift as long as well suited channel estimation algorithms are used. Especially, diversity is a powerful communication receiver technique that provides wireless link improvement with relative low cost. Unlike equalization, diversity requires no training overhead since the transmitter does not require the training sequence. Diversity exploits the random nature of radio propagation by finding independent (or at least high uncorrelated) signal paths for communication. Although it is not specified in European standard for DVB-T, more than one receive antenna can be used to achieve more robust reception by effectively combining the signals from the separate antennas. The improved reception can be leveraged to improve transmission reliability for both portable television sets and mobile televisions receivers.

As clock speed in communication systems pushes into the higher carrier frequency, phase noise and jitter are becoming increasingly critical to the system performance. Phase noise and jitter are different ways of quantifying the same phenomenon. Jitter is a measurement of the variations in the time domain, and essentially describes how far the signal period has wandered from its ideal value. On the other hand, phase noise is another measurement of variations in signal timing, but the results are displayed in the frequency domain. As far as OFDM is concerned, it is sensitive to the phase noise. In particular, the phase noise in the local oscillators of transmitter and receiver affects the orthogonality between the adjacent subcarriers and finally increases intercarrier interference (ICI) in an OFDM system. Therefore, it is important to exactly analyze the phase noise effect in an OFDM system. Given this trend, designers of high-speed digital equipment are beginning to pay greater attention to phase noise.

In this thesis, dual antennas, which are realized at the receiver side, incorporating the diversity scheme are utilized to achieve a substantial overall performance improvement over the conventional single technology in terms of the bit error rate

(BER), the achievable range, and link robustness. Moreover, phase noise compensation methods are proposed to increase the robustness system against phase noise and to provide a notable performance improvement.

This thesis is organized as follows. In Chapter 2, we describe that some concepts of receive diversity techniques are also included to provide a preliminary overview. Moreover, we describe the effects of phase noise and Doppler shift in an OFDM system. In Chapter 3, we build an OFDM-based DVB platform combining synchronization and channel estimation techniques. In Chapter 4, we introduce ideal diversity reception at different stages of the receiver and some phase noise compensation techniques suited to the OFDM-based DVB system. In Chapter 5, we conclude this thesis and propose some potential future works.

Chapter 2

Overview of Receive Diversity, Phase Noise, and Doppler Shift

Multiple antennas can be used for increasing the amount of diversity or the degrees of freedom in wireless communication systems. In addition, the effects of phase noise and Doppler shift are very important issues in wireless communications. In this chapter, we will introduce the basic features of receive diversity, the effects of phase noise and Doppler shift in OFDM systems.

2.1 Receive Diversity

In wireless communication systems, diversity techniques are widely used to mitigate the effects of multipath fading and enhance the reliability of transmission without increasing the transmitted power or sacrificing the bandwidth. The receive diversity techniques require multiple replicas of the transmitted signals at the receiver. The basic idea of receive diversity is that, if two or more independent samples of a signal are taken, these samples will fade in an uncorrelated manner, e.g. some samples are severely faded while others are less attenuated. This means that the probability of all samples being simultaneously below a given level is much lower than the probability of any individual sample being below that level. Thus, a proper combination of the various samples results in reducing severity of fading greatly, and improving reliability of transmission correspondingly. According to the domain where receive diversity is introduced, diversity techniques are classified into time diversity, frequency diversity and space diversity.

Time Diversity

Time diversity which results in uncorrelated fading signals at the receiver can be achieved by receiving messages in different time slots. The required time separation is at least the coherence time of the channel. The coherence time is a statistical measure of the period of time over which the channel fading process is correlated. In mobile communications, error control coding combines with interleaving to achieve time diversity. In this case, replicas of the transmitted signals are usually provided to the receiver in the form of redundancy in the time domain introduced by error control coding. The time separation between the replicas of the transmitted signals is provided by time interleaving results in decoding delays, and this technique is usually effective for fast fading environments where the coherence time of the channel is small. One of the drawbacks of the scheme is that due to the redundancy introduced in the time domain, there is a loss in bandwidth efficiency.

Frequency Diversity

In frequency diversity, a number of different frequencies are used to receive the same message. The frequencies need to be separated enough to ensure independent fading associated with each frequency. The frequency separation of the order of several times the channel coherence bandwidth will guarantee that the fading statistics for different propagation environments. In mobile communications, the replicas of the transmitted signals are usually provided to the receiver in the form of redundancy in the frequency domain introduced by spread spectrum such as multicarrier modulation. Spread spectrum techniques are effective when the coherence bandwidth of the channel is larger than the spreading bandwidth. Like time diversity, frequency diversity induces a loss in bandwidth efficiency due to a redundancy introduced in the frequency domain.

Space Diversity

Space diversity has been a popular technique in wireless communications. Space diversity is also called antenna diversity. It is typically implemented using multiple antennas or antenna arrays arranged together in space for reception. The multiple antennas are separated physically by a proper distance so that the individual signals are

uncorrelated. Typically, a separation of a few wavelengths is enough to obtain uncorrelated signals. In space diversity, the replicas of the transmitted signals are usually provided to the receiver in the form of redundancy in the space domain. Unlike time and frequency diversity, space diversity does not induce any loss in bandwidth efficiency. This property is very attractive for future high data rate in wireless communications.

In essence, multiple copies of the transmitted stream are received, which can be efficiently combined using appropriate signal processing algorithms. This technique is aimed to provide an AWGN-like channel where the outage probability is driven to zero as the number of antennas increases. There are several ways to combine the received signals, such as switch combining, selective combining, equal gain combining, and maximal ratio combining (MRC). In the following, we will describe the MRC scheme to present the concept of optimal combining. In the MRC scheme, the outputs of the N_r receive antennas are linearly combined so as to maximize the instantaneous signal-to-noise ratio (SNR). The coefficients that yield the maximum SNR can be found from the optimization theory. Consider a $1\times N_r$ transmission scheme and denote the received data at the lth receive antenna as

$$y^{(l)} = h^{(l)}x + n^{(l)} \tag{2.1}$$

where $h^{(l)}$ denotes the channel gain from the transmit antenna to the lth receive antenna, and $n^{(l)}$ is the independent noise sample of power σ^2. Further, we assume perfect channel estimation at the receive side. Finally, the transmitted signal power is normalized to be 1. The MRC scheme is achieved by using the linear combination

$$y = \sum_{l=1}^{N_r} w^{(l)*} y^{(l)} = \sum_{l=1}^{N_r} w^{(l)*} h^{(l)} x + \sum_{l=1}^{N_r} w^{(l)*} n^{(l)} \tag{2.2}$$

The noise power after MRC in (2.2) is given by

$$\varsigma_n = \sigma^2 \sum_{l=1}^{N_r} \left| w^{(l)} \right|^2 \tag{2.3}$$

while the instantaneous signal power is

$$\sum_{l=1}^{N_r} \left| w^{(l)*} h^{(l)} \right|^2 \tag{2.4}$$

The output SNR of the MRC expressed by

$$\gamma = \frac{\sum_{l=1}^{N_r} \left| w^{(l)*} h^{(l)} \right|^2}{\sigma^2 \sum_{l=1}^{N_r} \left| w^{(l)} \right|^2} \tag{2.5}$$

can be maximized by applying the Cauchy-Schwartz inequality defined as

$$\sum_{l=1}^{N_r} \left| a^{(l)*} b^{(l)} \right|^2 \le \sum_{l=1}^{N_r} \left| a^{(l)} \right|^2 \sum_{l=1}^{N_r} \left| b^{(l)} \right|^2 \tag{2.6}$$

where the equality in (2.6) holds for $w^{(l)} = h^{(l)}$ for all *l*, which provides the weighting coefficients for MRC. This means that the heavily faded antennas, which are less reliable, are counted less than the less faded antennas, which are more reliable, and vice versa. Substituting $w^{(l)} = h^{(l)}$ into (2.5) leads to the SNR of MRC given by

$$\gamma_{MRC} = \frac{1}{\sigma^2} \sum_{l=1}^{N_r} \left| w^{(l)} \right|^2 \tag{2.7}$$

Noting that $|w^{(l)}|^2 / \sigma^2$ is the post-processing SNR for the *l*th receive antenna, and (2.7) is just the sum of the SNRs for each receive antenna, which means γ_{MRC} can be large even when the individual SNRs are small. It can also be proved that the MRC is the optimal combining technique in the sense of MMSE [25]. In Chapter 4, we will compare various receive diversity schemes in detail.

2.2 Phase Noise Phenomenon

The time-domain behavior of phase noise effects introduced by the local oscillator in any receiver is called jitter, which is defined as the variation in the time of the significant instants such as zero crossings, as shown in Fig. 2.1. Alternatively, jitter is the deviation of each period from the ideal value as shown in Fig. 2.2. Since phase noise is the Fourier Transform of the jitter introduced by random Gaussian noise, phase noise may be modeled as Wiener process [13]. Phase noise can be interpreted as a parasitic phase modulation in the oscillator's signal, which ideally would be a unique carrier with constant amplitude and frequency [14]. It has been modeled for simulation purposes as a phase modulation of the subcarrier. The modulated signal is a zero mean white Gaussian random process $\phi_W(n)$ with variance σ_W^2. The corresponding

autocorrelation function is given by

$$R_{\phi_W}(k) = \sigma_W^2 \bullet \delta(k) \tag{2.8}$$

And its power spectral density is given by

$$S_{\phi_W}(f) = \sum_{k=-\infty}^{\infty} R_{\phi_W}(k) \bullet e^{-j2\pi fk} = \sigma_W^2 \tag{2.9}$$

It has been lowpass filtered with an impulse response $h_{LPF}(n)$, so that its power spectral density becomes

$$S_\phi(f) = S_{\phi_W}(f) \bullet \left|H_{LPF}(f)\right|^2 \tag{2.10}$$

where $H_{LPF}(f)$ denotes the Fourier Transform of $h_{LPF}(n)$. In (2.10), $S_\phi(f)$ is the power spectral density of phase noise and is modeled as Wiener process generated by Gaussian process passing through the lowpass filter as Fig. 2.3. Phase noise variance is also used as a parameter that will be easy to relate to commonly used phase noise specifications.

2.2.1 Theoretical Analysis of Phase Noise in OFDM Systems

For the sake of simplicity, we will not consider the cyclic prefix and assume that the channel is flat. Therefore, the signal only affected by phase noise $\phi(n)$ at the receiver is given by

$$y(n) = x(n) \bullet e^{j\phi(n)} \tag{2.11}$$

In order to separate the signal and phase noise terms, let us suppose that $\phi(n)$ is small, so that

$$e^{j\phi(n)} \approx 1 + j\phi(n) \tag{2.12}$$

After FFT, the transformed signal is given by

$$Y_k = X_k + \frac{j}{N}\sum_{r=0}^{N-1} X_r \sum_{n=0}^{N-1} \phi(n) e^{j(2\pi/N)(r-k)n} = X_k + \varepsilon_k \tag{2.13}$$

where N is the number of subcarriers, the suffix k denotes the kth tone in one OFDM symbol and error term ε_k for each tone resulting from some combination of all of them is added to the useful signal. Let us analyze more deeply this phase noise contribution:

(1). If $r = k$: common phase error (CPE)

$$\varepsilon_k = \frac{j}{N} X_k \sum_{n=0}^{N-1} \phi(n) = j \bullet X_k \bullet \Phi \tag{2.14}$$

We have a common error added to every tone that is proportional to its value multiplied by a complex number $j\Phi$, which is a rotation of the constellation given by

$$\Phi = \frac{1}{N} \sum_{n=0}^{N-1} \phi(n) \tag{2.15}$$

Since this rotation is identical for all the subcarriers, the phase difference between consecutive symbols can be obtained with the aid of pilots induced in the OFDM frame and corrected.

(2). If $r \neq k$: ICI

$$\varepsilon_k = \frac{j}{N} \sum_{\substack{r=0 \\ r \neq k}}^{N-1} X_r \sum_{n=0}^{N-1} \phi(n) e^{j(2\pi/N)(r-k)n} \tag{2.16}$$

This term corresponds to the summation of the information of the other $N-1$ subcarriers multiplied by some complex number which comes from an average of phase noise with a spectral shift. This result is also a complex number that is added to each subcarrier's useful signal and has the appearance of Gaussian noise. It is normally known as ICI or loss of orthogonality.

2.3 Doppler Shift

The relative motion between the base station and the mobile results in random frequency modulation due to different Doppler shifts on each of the multipath components [25]. Doppler shift will be positive or negative depending on whether the mobile receiver is moving toward or away from the base station. Consider a mobile moving at a constant velocity *v*, along a path segment having length *d* between points X and Y, while it receives signals from a remote source S, as illustrated in Fig. 2.4. The difference in path length traveled by the wave from source S to the mobile at points X and Y is $\Delta l = d\cos\theta = v\Delta t\cos\theta$, where Δt is the time required for the mobile to travel from X to Y, and θ is assumed to be the same at points X and Y since the source is assumed to be very far away. The corresponding phase change in the received

signal can be expressed by

$$\Delta\phi = \frac{2\pi\Delta l}{\lambda} = \frac{2\pi v\Delta t}{\lambda}\cos\theta \tag{2.17}$$

According to (2.17), the apparent change in frequency, or Doppler shift, denoted by f_d, is given by

$$f_d = \frac{1}{2\pi}\bullet\frac{\Delta\phi}{\Delta t} = \frac{v}{\lambda}\bullet\cos\theta \tag{2.18}$$

It can be seen from (2.17) that if the mobile is moving toward the direction of arrival of the wave, Doppler shift is positive, and if the mobile is moving away from the direction of arrival of the wave, Doppler shift is negative. Thus, we can understand that Doppler shift increases the signal bandwidth.

2.3.1 Theoretical Analysis of Doppler Shift in OFDM Systems

In mobile radio environment, the channel impulse response model for one data block is expressed as

$$h(n) = \sum_{l=0}^{M-1} h_l e^{j\frac{2\pi}{N}\varepsilon_l(n-n_l)} \tag{2.19}$$

where M denotes the total number of propagation paths, and n_l and $\varepsilon_l = f_{d_l}/\Delta f$, with Δf being the subcarrier separation, are the delay chip number and the normalized frequency offset associated with the lth path, respectively [26]. For each path, the amplitude of h_l is Rayleigh distributed. Since the spectral behavior of OFDM is more important than the temporal behavior of the time domain, the analysis of the frequency domain representation of the channel response is preferred. Consider one typical path and the channel impulse response of the lth path can be expressed by

$$h_l(n) = h_l e^{j\frac{2\pi}{N}\varepsilon_l(n-n_l)} \tag{2.20}$$

Therefore, the corresponding frequency domain response at the kth subcarrier can be obtained by FFT as below

$$H_{l,k} = \frac{1}{N}\sum_{n=0}^{N-1} h_l e^{j\frac{2\pi}{N}\varepsilon_l(n-n_l)} e^{-j\frac{2\pi}{N}nk} = \frac{1}{N} h_l e^{-j\frac{2\pi}{N}\varepsilon_l n_l}\sum_{n=0}^{N-1} e^{-j\frac{2\pi}{N}n(k-\varepsilon_l)} \tag{2.21}$$

Then, the received frequency domain signal $Y_{l,k}$ is given by

$$\begin{aligned} Y_{l,k} &= \frac{1}{N} h_l X_k e^{-j\frac{2\pi}{N}\varepsilon_l n_l} \sum_{n=0}^{N-1} e^{-j\frac{2\pi}{N}n(k-\varepsilon_l)} \\ &= \frac{1}{N} h_l \delta(k-r) e^{-j\frac{2\pi}{N}\varepsilon_l n_l} \sum_{n=0}^{N-1} e^{-j\frac{2\pi}{N}n(k-\varepsilon_l)} \\ &= \frac{1}{N} h_l e^{-j\frac{2\pi}{N}\varepsilon_l n_l} \sum_{n=0}^{N-1} e^{-j\frac{2\pi}{N}n(k-r-\varepsilon_l)} \end{aligned} \tag{2.22}$$

Note that the second equation holds due to that the transmitted data is set to be $X_k = \delta(k-r)$ for $0 \le r < N$. Let us analyze more deeply this Doppler shift contribution:

(1). If $r = k$: CPE and frequency offset

$$Y_{l,k} = \frac{1}{N} h_l \underbrace{e^{-j\frac{2\pi}{N}\varepsilon_l n_l}}_{\text{CPE}} \underbrace{\sum_{n=0}^{N-1} e^{j\frac{2\pi}{N}n\varepsilon_l}}_{\text{Frequency offset}} \tag{2.23}$$

(2). If $r \neq k$: ICI

$$Y_{l,k} = \frac{1}{N} h_l e^{-j\frac{2\pi}{N}\varepsilon_l n_l} \sum_{\substack{n=0 \\ k \neq r}}^{N-1} e^{-j\frac{2\pi}{N}n(k-r-\varepsilon_l)} \tag{2.24}$$

Therefore, Doppler shift results in three effects which are CPE, frequency offset and ICI.

2.4 Summary

In wireless communication systems, diversity is a powerful technique for the improvement of system performance. Several types of diversity have already been introduced. In addition, the effects of phase noise and Doppler shift are investigated in OFDM systems. Based on the concepts mentioned above, we will propose diversity reception and phase noise compensation schemes for DVB-T systems in Chapter 4.

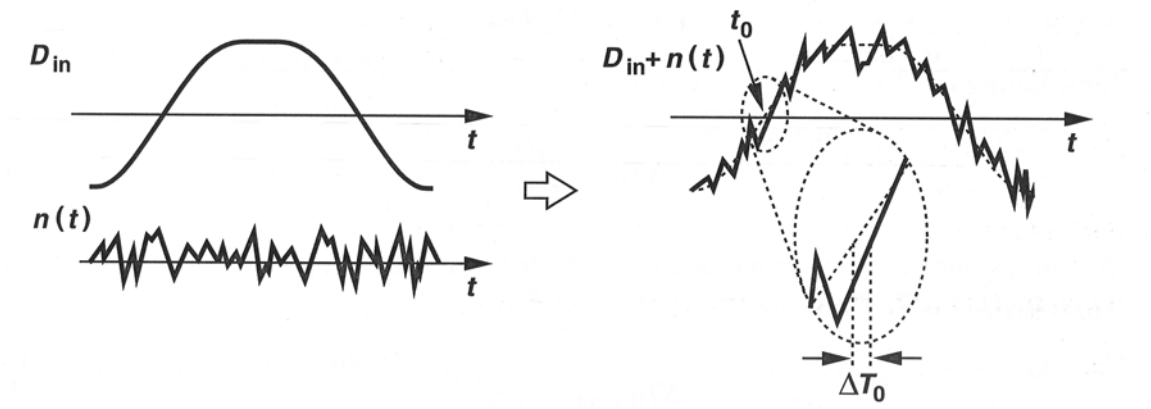

Figure 2.1: Illustration of jitter induced by additive noise.

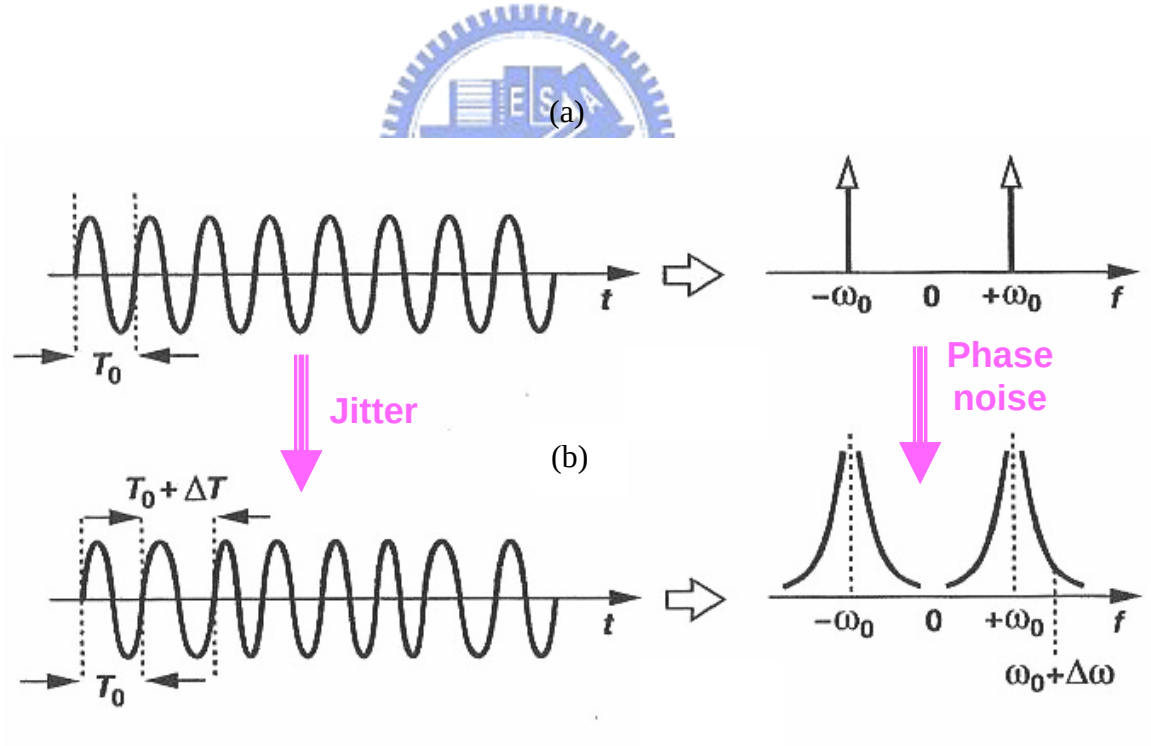

Figure 2.2: Illustration of relation between jitter and phase noise. (a) Influence of jitter on signal duration. (b) Influence of phase noise on signal bandwidth.

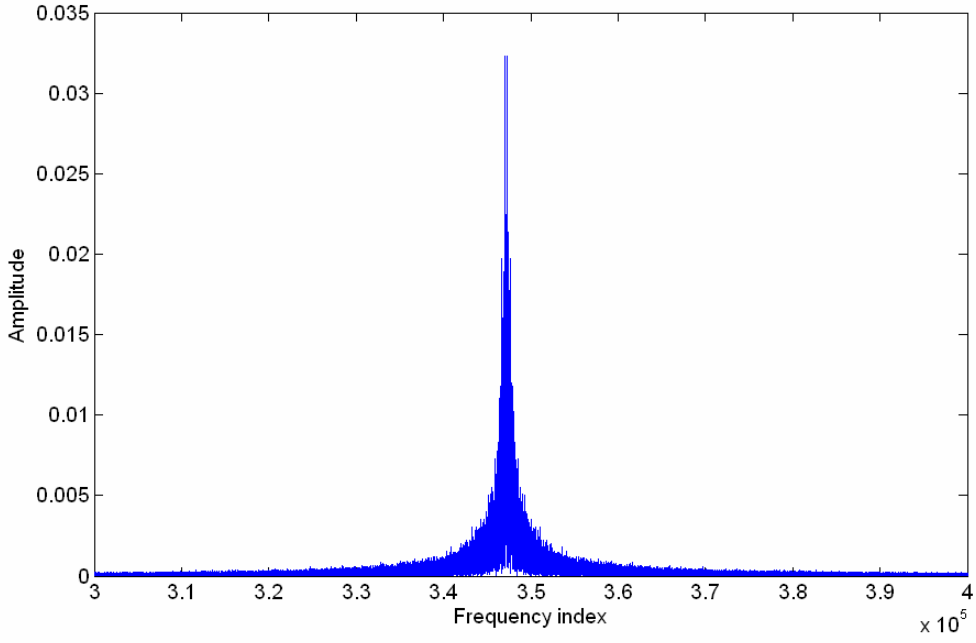

Figure 2.3: Modeling phase noise in frequency domain.

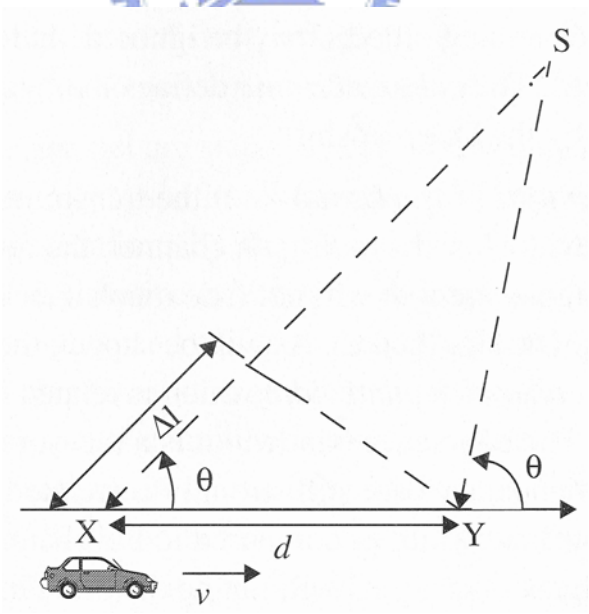

Figure 2.4: Illustration of Doppler shift.

Chapter 3

OFDM-Based DVB System

DVB system incorporating the OFDM technique can promise robustness against intersymbol interference (ISI) and efficiency in spectrum utilization. Specifically, OFDM with error correcting coding technique used, frequently referred to as COFDM modulation, is a key ingredient of DVB-T system. In this chapter, we will present some possible schemes of the DVB-T system and show how a DVB-T system benefits from the corresponding scheme. Furthermore, the design tradeoff of the DVB-T system is also included.

3.1 Review of OFDM

OFDM can be regarded as either a modulation or a multiplexing technique. The basic concept of OFDM is to split a high rate data stream into a number of lower rate streams that are transmitted simultaneously over subcarriers [27]-[28]. In order to eliminate the effect of ISI, each OFDM symbol consists of a guard time, which is chosen to be larger than the maximum delay spread such that the current OFDM symbol never hears the interference from the previous one. However, this will cause ICI due to the loss of orthogonality between subcarriers. As a remedy, OFDM symbols are cyclically extended in the guard time to introduce cyclic prefix, as shown in Fig. 3.1. This ensures that the delayed replicas of an OFDM symbol always have an integer number of cycles within the FFT interval. Consequently, cyclic prefix can successively resolve both ISI and ICI caused by multipath as long as the delay spread of channel is smaller than the length of cyclic prefix. In addition, insertion of cyclic prefix makes the

transmitted OFDM symbol periodic, leading to that the linear convolution processing applied to the transmitted OFDM symbols (containing cyclic prefix) and channel impulse response will be translated into a circular convolution one. According to discrete-time linear system theory, the frequency response associated with the output of a circular convolution is equivalent to the product of the frequency responses associated with the OFDM symbol and channel.

Definitely, OFDM is a powerful modulation technique for increments in bandwidth efficiency and simplification in removal of distortion due to a multipath channel. Advances in fast Fourier transform (FFT) algorithm enable OFDM to be efficiently implemented in hardware, even for a large number of subcarriers. The key advantages of OFDM transmission are summarized as follows:

1. OFDM can effectively deal with multipath delay channels with much lower implementation complexity as compared with that of a single carrier system using an equalizer.
2. OFDM can achieve robustness against impulse noise because it possesses a long symbol period compared with an equal data-rate single-carrier system.
3. OFDM can support dynamic bit loading technique, in which different subcarriers use different modulation modes depending on the channel characteristic or the noise level. Hence, the system performance can be significantly enhanced in this systematic way.

3.2 Overview of DVB-T Systems

The DVB organization was formed in September 1993. Along these years, several system specifications have been proposed and become standard in the European Telecommunication Standard Institute (ETSI) or European Committee for Electrotechnical Standardisation. The term “OFDM-based DVB” system is often rewritten by the “DVB-T” system. The DVB-T system for terrestrial broadcasting is probably the most complex DVB delivery system. The key feature of this system is the employment of COFDM, which is a very flexible wide-band multicarrier modulation system using different levels of forward error correction, time and frequency interleaving and two level hierarchical channel coding [23]-[24]. Basically, the

transmitted information is split into a given number (“2k” 1705 or “8k” 6817) of modulated carriers with individual low bit rate, so that the corresponding symbol time becomes larger than the delay spread of the channel. A guard interval (1/4, 1/8, 1/16, 1/32 of the symbol duration) is inserted between successive symbols to avoid ISI and to protect against echoes. Depending on the channel characteristics, different parameters (subcarrier modulation: QPSK, 16QAM, and 64QAM; number of carriers: 2k and 8k; code rate of inner protection, and guard interval length) can be selected leading to different operation modes. Every mode offers a trade-off between net bit rate and protection of the signal (against fading, echoes, etc.). Depending on the selected operation mode, 60 different net bit rates could be obtained ranging from 5 to 32 Mbps. The selection of the COFDM modulation system presents two major advantages that make its use very interesting to terrestrial digital video broadcasting:

1. COFDM improves the ruggedness of the system in the presence of artificial (long distance transmitters) or natural (multiple propagation) echoes. The echoes may benefit instead of interfering the signal if they fall inside the guard interval.
2. COFDM provides a considerable degree of immunity to narrow-band interferers as maybe considered the analogue TV signals; and on the other hand it is seen by those analogue signals as white noise, therefore not interfering or having little effect upon them.

These characteristics enable a more efficient use of the spectrum and the introduction of single frequency networks (SFN). Furthermore, some characteristics of a DVB-T system, as shown in Fig. 3.2, will be discussed as below.

3.2.1 Scrambler

This is a method of removing long runs of 0’s or 1’s in the signal which would otherwise give the receiver a problem at the other end of the channel. This is achieved at the bit level. The pseudo random sequences produced from the incoming bit stream are generated by the polynomial given by

$$1 + x^{14} + x^{15} \tag{3.1}$$

This is realized, as shown Fig. 3.3, with a shift register. Bits 14 and 15 are fed into an XOR gate, then back to the input and also XOR’ed with the data, when enabled, to give

the output. The initialization sequence is loaded every 8 transport packets. Note that this gives a pseudo random binary sequence (PRBS).

3.2.2 Outer Coder (Reed-Solomon Coder)

Reed-Solomon (RS) coding is mathematically very complicated and will not be explained here in any detail. The aim here is simply to give an overview of the coding technique. The coding is a block level code, i.e., it operates over a block of data. The block of data must therefore be constructed prior to the code operation. This puts an overhead on the system in terms of memory and the need for block synchronization. The coding adds 16 additional bytes to the 188 byte transport stream packets, making a final transport stream packet size of 204 bytes. This error correction algorithm, as applied to a transport stream, is characterized by the three numbers *n*, *k* and *l*, where *n* is the number of bytes in the final transport stream, *k* is the number of bytes of the original transport stream, and *t* is the number of bytes that can be corrected. We set the parameters to be $n = 204$, $k = 188$, and $t = 8$. This is referred to as RS (204, 188, 8) shortened code. The RS code effectively specifies a polynomial by generating a large number of points. The RS code can detect and correct up to $(n-k)/2$ errors. The field generator polynomial is used as

$$P(x) = x^8 + x^4 + x^3 + x^2 + 1 \tag{3.2}$$

with the code generator polynomial as below

$$G(x) = (x + \alpha^0)(x + \alpha^1)\cdots(x + \alpha^{15}) \tag{3.3}$$

3.2.3 Outer Interleaver (Convolutional Interleaver)

Interleaving is a form of time diversity that is employed to disperse bursts of errors in time. A sequence of data symbols is interleaved before transmission over a bursty channel. If errors occur during transmission, reshaping the original sequence to its original ordering has the effect of spreading the error over time. By spreading the data symbols over time, it is possible to use channel coding, such as RS coding in DVB-T systems, which protects the data symbols from corruption by channel. The interleaver performance depends on the required memory for data storage and the delay in interleaving and deinterleaving, which should be kept as small as possible. In [23],

we obtain that the delay with convolutional interleaver is half the operation time compared with block interleaver and an efficiency of 14.2% for block interleaver and 64% for convolutional interleaver, where efficiency can be defined as the ratio of the length of the smallest burst of errors that can cause the errors correcting capability of the code to be exceeded to the number of memory element used in the interleaver. As stated above, the convolutional interleaver is applied in the outer interleaver of a DVB-T system. The outer coding can correct up to 8 bytes in a transport stream packet. Clearly, if a burst error condition occurs, i.e. a burst of energy from some noise source, then more than 8 bytes within the same packet could become corrupted. The convolution effectively takes these errors and spreads them out over a number of packets, thus allowing the outer coding to be more effective. Fig. 3.4 shows the outer interleaver and deinterleaver. Data is input from the RS outer coding and output to the convolution inner coder. Therefore, there are 12 individual branches with the largest first-input first-output (FIFO) being of length 187 bytes. Input bytes will therefore be delay by 17, 34, 51, …, 187 bytes, depending on the byte index. Fig. 3.5 shows the data format of passing though the scrambler, outer coder and interleaver.

3.2.4 Inner Coder (Convolutional Coder)

Convolutional coding operates at the bit level rather than block level such as RS coding. This has the advantage of the generator not having to store a whole block of data in expensive memory prior to performing the coding. The input stream is fed into shift register stages which have intermediate output taps after each stage. The input stream and various output taps are modulo two added. The DVB-T system actually uses 6 shift register stages and the generator polynomials are shown as

$$\begin{aligned} G_1 &= 171_{\text{Oct}} \\ G_2 &= 133_{\text{Oct}} \end{aligned} \tag{3.4}$$

The architecture as shown in Fig. 3.6 can be considered a state machine. Since there are 6 stages in the DVB-T implementation, this gives rise to 64 states. It is the change from one state to another based on which we can draw the trellis diagram to be applied in the Viterbi decoding algorithm.

3.2.5 Inner Interleaver

Inner interleaver is also performed to basically spread out the errors and so make the inner coding more effective. The inner interleaving consists of bit-wise interleaving followed by symbol interleaving. Both the bit-wise interleaving and the symbol interleaving processes are block-based.

Bit-Wise Interleaver

The input, which consists of up to two bit streams, is demultiplexed into *v* sub-streams, where *v* = 2 for QPSK, *v* = 4 for 16QAM, and *v* = 6 for 64QAM in Fig. 3.7. The block size is the same for each interleaver, but the interleaving sequence is different in each case. The bit interleaving block size is 126 bits. The block interleaving process is therefore repeated exactly twelve times per OFDM symbol of useful data in the 2k mode and forty-eight times per symbol in the 8k mode. For each bit interleaver, the input bit vector is defined by

$$B(e) = (b_{e,0},\ b_{e,1},\ b_{e,2},\ ...,\ b_{e,125}) \tag{3.5}$$

where $b_{e,w}$ denotes the bit number *w* of inner bit interleaver *e*, $B(e)$ denotes the input vector to inner bit interleaver *e*, and *e* ranges from 0 to *v*-1. The interleaved output $A(e) = (a_{e,0},\ a_{e,1},\ a_{e,2},\ ...,\ a_{e,125})$ is defined by

$$a_{e,w} = b_{e,He(w)},\quad w = 0,\ 1,\ 2,...,\ 125 \tag{3.6}$$

where $a_{e,w}$ denotes the bit number *w* of inner bit interleaver output stream *e*, and $H_e(w)$ is a permutation function which is different for each interleaver. The $H_e(w)$ is defined as follows for each interleaver

$$\begin{aligned}
&\text{I0: } H_0(w) = w \\
&\text{I1: } H_1(w) = (w+63) \bmod 126 \\
&\text{I2: } H_2(w) = (w+105) \bmod 126 \\
&\text{I3: } H_3(w) = (w+42) \bmod 126 \\
&\text{I4: } H_4(w) = (w+21) \bmod 126 \\
&\text{I5: } H_5(w) = (w+84) \bmod 126
\end{aligned} \tag{3.7}$$

The outputs of the *v* bit interleavers are grouped to form the digital data symbols, such that each symbol of *v* bits will consist of exactly one bit from each of the *v* interleavers.

Hence, the output from the bit-wise interleaver is a *v* bit word *y'*, i.e.

$$y'_w = (a_{0,w},\ a_{1,w},...,\ a_{v\text{-}1,w}) \tag{3.8}$$

Symbol Interleaver

The purpose of the symbol interleaver is to map the 2, 4 or 6 bit words onto one of the OFDM carriers (1512 for 2k mode or 6048 for 8k mode). The interleaved vector $Y = (y_0,\ y_1,\ y_2,\ ...y_{N_{\max}-1})$ is defined by

$$\begin{aligned} y_{H(q)} &= y'_q \quad \text{for even symbols for } q=0,..., N_{\max}-1 \\ y_q &= y'_{H(q)} \quad \text{for odd symbols for } q=0,..., N_{\max}-1 \end{aligned} \tag{3.9}$$

where $N_{\max} = 1512$ in the 2k mode and $N_{\max} = 6048$ in the 8k mode. $H(q)$ is a permutation function defined by the following. An $(N_r - 1)$ bit binary word R'_i is defined, with $N_r = \log_2 M_{\max}$, where $M_{\max} = 2048$ in the 2k mode and $M_{\max} = 8192$ in the 8k mode, where R'_i takes the following values:

$$\begin{aligned} &i = 0,1:\ R'_i[N_r - 2,\ N_r - 3,\ ...,\ 1,\ 0] = 0,\ 0,...,\ 0,\ 0 \\ &i = 2:\ R'_i[N_r - 2,\ N_r - 3,\ ...,\ 1,\ 0] = 0,\ 0,...,\ 0,\ 1 \\ &2 < i < M_{\max}: \\ &\{\ R'_i\ [N_r - 3,\ N_r - 4,...,\ 1,\ 0] = R'_{i-1}[N_r - 2,\ N_r - 3,...,\ 2,\ 1]; \\ &\quad \text{2K mode}:\ R'_i[9] = R'_{i-1}[0] \oplus R'_{i-1}[3] \\ &\quad \text{8K mode}:\ R'_i[11] = R'_{i-1}[0] \oplus R'_{i-1}[1] \oplus R'_{i-1}[4] \oplus R'_{i-1}\ [6]\ \} \end{aligned} \tag{3.10}$$

A vector R_i is derived from the vector R'_i by the bit permutations given in Table 3.1. The permutation function $H(q)$ is defined by the following algorithm

$$\begin{aligned} &q = 0; \\ &\text{for } (i = 0;\ i < M_{\max};\ i = i + 1) \\ &\{\ H(q) = (i\ \bmod 2) \times 2^{N_r - 1} + \sum_{j=0}^{N_r - 2} R_i(j) \cdot 2^j; \\ &\quad \text{if } (H(q) < N_{\max}),\ q = q + 1;\ \} \end{aligned} \tag{3.11}$$

A schematic block diagram of the algorithm used to generate the permutation function is represented in Fig. 3.8 for the 2k mode

3.2.6 Subcarrier Modulation Mapping and OFDM Frame Structure

The system uses OFDM transmission. All data carriers in one OFDM frame are modulated using either QPSK, 16QAM, 64QAM, non-uniform 16QAM or non-uniform 64QAM constellations. The exact values of the constellation points are given by

$$d = K_{MOD} \times (n + jm) \tag{3.12}$$

where K_{MOD} is the normalization factor and $z \in \{n + jm\}$ with values of n, m is given by Table 3.2. The basic structure of what is known as an OFDM signal is a variable number of frequency carriers, either 1705 (known as 2k mode) or 6817 (known as 8k mode) as Table 3.3. These carriers are spaced in such a way as to allow them to fit into the 7.61 MHz bandwidth. These carriers can be shown in Fig. 3.9 and described as follows.

1. Data: with a variable number of bits per carrier
2. Transmission parameter signalling (TPS): transmission information
3. Pilot: for receive synchronization, there are two types both transmitted at boosted power levels
   a. Continual: there are 177 tones in 8k mode, and 45 tones in 2k mode. These always are at the same frequency in different OFDM symbols. These pilots are used to compute the CPE. The CPE is an error that is introduced into the signal due to the local oscillator's phase noise. The CPE is a change in phase of all carriers within an OFDM symbol compared to the next OFDM symbol.
   b. Scattered: there are 524 tones in 8k mode, and 131 tones in 2k mode. Specified insertion pattern within the symbol. These pilots are used to estimate the channel distortion.

On the other hand, the guard interval is a replication of the end of the symbol and is added to the beginning of the symbol. The guard interval length of DVB-T system can be 1/4, 1/8, 1/16 or 1/64 of the symbol duration. There are two main reasons for the insertion of a guard interval. The first one is to combat against the ISI. The other is to allow the receiver to identify the start of a symbol. Finally, Table 3.4 gives simulated BER performance anticipating "perfect channel estimation and no phase noise" for various combinations of channel coding and modulations.

3.3 Synchronization in DVB-T Systems

One of the major drawbacks of an OFDM system is its high sensitivity to synchronization errors, in particular, to carrier frequency errors. In an OFDM system, the pilot or cyclic prefix is used for the sake of synchronizing OFDM signals. An algorithm with the pilot used, referred to as the pilot-based synchronization, is developed based on a two-stage procedure. First, the transmitter encodes a number of reserved subchannels with the given phases and amplitudes. A correlation detector is then performed on the received signal to extract the synchronization information at the pilot tones. On the other hand, a scheme with the cyclic prefix used, referred to as the cyclic-prefix-based synchronization, can enable the self-synchronization [28]. The block diagram of synchronization techniques in DVB-T systems is illustrated in Fig. 3.10. The corresponding function of each block is investigated as below.

3.3.1 Coarse Timing and Frequency Offset Estimation

Fig. 3.11 shows a cyclic-prefix-based synchronizer for coarse timing and frequency offset estimation [29]. The cyclic prefix generated by duplicating the last N_{cp} samples of the N_c-sample OFDM symbol is prefixed in the $(N_c + N_{cp})$-sample OFDM symbol. Note that the duration of the cyclic prefix should be greater than the maximum delay of the channel impulse response to eliminate ISI. Since the receiver cannot obtain the symbol starting position within the observation interval preliminarily, a likelihood function based on the consecutive samples of the received OFDM signal y along with moving average at time instant i is suggested for coarse timing synchronization and is given by

$$\hat{j} = \arg\max_{j} \left\{ \left| \sum_{i=0}^{N_{cp}-1} y^*(j+i-N_c) y(j+i) \right| \right\} \tag{3.13}$$

where $\hat{j}$ and $y(i)$ denote the estimated symbol starting position and the ith sample of the received OFDM signal. In addition, frequency offset estimation is given by

$$f_{\text{coarse}} = \frac{1}{2\pi N_c T_{sample}} \arg\left\{ \sum_{i=0}^{N_{cp}-1} y^*(\hat{j}+i-N_c) y(\hat{j}+i) \right\} \tag{3.14}$$

where T_{sample} denotes the sample duration. Since coarse timing and frequency offset estimates in (3.13) and (3.14), respectively, are usually distorted due to noise effect, we can average the estimates over several successive OFDM symbols to enhance the accuracy in timing and frequency offset estimation.

3.3.2 Fine Timing Estimation

Performance of coarse timing estimation will degrade due to the channel random noise, which will induce the estimation error of one or two samples. Therefore, a fine timing estimator is necessary for enhancing its robustness against noise. Specifically, as the starting position estimate $\hat{j}$ is obtained, we correlate totally 7 OFDM symbols before and after $\hat{j}$ with known continual pilots of the DVB-T system. The exact symbol starting position can be determined by maximizing the correlator output. Mathematically speaking, the algorithm, referred to as an early-late fine timing estimation, is given by

$$\tilde{j} = \max_{j} \left\{ \left| \sum_{k=1}^{N_{p,cont}} Y_k^* (\hat{j} + j) \cdot X_{k,cont} \right| \right\}, \quad j = -3, -2, \cdots, 2, 3 \tag{3.15}$$

where $\tilde{j}$ is the estimated fine time index, $N_{p,cont}$ is the number of the continual pilots, and $X_{k,cont}$ is the value of the kth continual pilot, with k being the frequency index.

3.3.3 Fine Frequency Estimation

In order to further improve the performance in frequency offset estimation, a fine frequency offset estimator, as shown in Fig. 3.12, is constructed based on the continual pilots $X_{k,cont}$ and given by

$$f_{fine} = \frac{1}{2\pi (N_c + N_{cp}) T_{sample}} \arg \left\{ \sum_{k=1}^{N_{p,cont}} X_{k+N_c,cont} X_{k,cont}^* \right\} \tag{3.16}$$

Similarly, several OFDM symbols can be used to enhance the accuracy in timing and frequency offset estimation [30].

3.3.4 Frame Timing Estimation

Generally, the receiver performs the timing estimation at the beginning of the reception [31]. However, clock offset may cause sample drifting during one frame duration. Therefore, frame timing synchronization is necessary for every frame. Substantially, the second to 17 bits of the TPS pilot can be used to estimate frame starting position and the corresponding likelihood function for frame timing synchronization is given by

$$\hat{j} = \max_{j} \left\{ \left| \sum_{k=1}^{N_{p,TPS}} Y_k^*(j) \cdot X_{k,TPS} \right| \right\} \tag{3.17}$$

where $N_{p,TPS}$ denotes the number of bits associated with the TPS pilot for frame synchronization, and $X_{k,TPS}$ denotes the TPS pilot. The frame timing estimation in (3.17) possesses two advantages: one is that the TPS pilot is more reliable due to the extra protection of the Bose-Chaudhuri-Hocquenghem (BCH) coding. The other is that we only need 16 synchronization bits in one frame, leading to a reduction of computational complexity.

3.4 Channel Estimation in DVB-T Systems

In wideband mobile communication systems, under the assumption of a slow fading channel, in which the channel transfer function is stationary within several OFDM data symbols, preambles or training sequences can be used to estimate the channel response for the following OFDM data symbols. However, in practice, the channel response may significantly vary even within one OFDM data block. Therefore, in DVB-T systems, it is preferable to estimate the channel characteristic based on the pilot signals in each individual OFDM data block. The conventional channel estimation involves a two-stage procedure. First, the channel responses associated with the pilot tones are estimated. Second, interpolation technique is used to obtain channel responses of the data tones. We will introduce two pilot-aided channel estimation methods. One is least square (LS) channel estimation, together with piecewise-linear interpolation. The other is application of low-pass filtering on the transformed pilot tones to reduce the Gaussian noise and ICI effects.

3.4.1 Least Square Channel Estimation with Linear Interpolation

Consider an OFDM system with $N_{p,scat}$ scattered pilot signals. The received pilot signal in vector form can be given by

$$\begin{aligned}\mathbf{Y}_{scat} &= \mathbf{X}_{scat}\mathbf{H}_{scat} + \mathbf{N}_{scat} \\ &= \underbrace{\begin{bmatrix} X_{scat}(0) & & 0 \\ & \ddots & \\ 0 & & X_{scat}(N_{p,scat}-1) \end{bmatrix}}_{\mathbf{X}_{scat}} \underbrace{\begin{bmatrix} H_{scat}(0) \\ \vdots \\ H_{scat}(N_{p,scat}-1) \end{bmatrix}}_{\mathbf{H}_{scat}} + \mathbf{N}_{scat}\end{aligned} \tag{3.18}$$

where $\mathbf{X}_{scat}$, $\mathbf{H}_{scat}$, and $\mathbf{N}_{scat}$ denote the scattered pilot signals, the corresponding channel responses, and the noise, respectively [32]. According to the LS criterion, the channel transfer function can be obtained by

$$\arg\min_{\mathbf{H}_{scat}} \left\| \mathbf{Y}_{scat} - \mathbf{X}_{scat}\mathbf{H}_{scat} \right\|^2 \tag{3.19}$$

whose solution is given by

$$\widehat{\mathbf{H}}_{scat,LS} = \mathbf{X}_{scat}^{-1}\mathbf{Y}_{scat} \tag{3.20}$$

From (3.20), the channel estimate can be obtained by dividing the received signals by the known scattered pilots. This implies that the LS channel estimator is easier to implement. As the estimation of the channel transfer functions of pilot tones is determined, the channel responses of data tones are then constructed by the linear interpolation technique. Note that we consider a linear interpolation method due to simplicity. With the linear interpolation used, two successive pilot subcarriers are used to compute the channel responses of data subcarriers located between these two pilot tones. Mathematically speaking, the estimated channel response of data subcarrier l within the m th and $(m+1)$ th pilot tones is given by

$$\begin{aligned}\widehat{H}(mL+l) &= (1-\frac{l}{L})\widehat{H}_{scat}(m) + \frac{l}{L}\widehat{H}_{scat}(m+1) \\ &= \widehat{H}_{scat}(m) + \frac{l}{L}\left(\widehat{H}_{scat}(m+1) - \widehat{H}_{scat}(m)\right), \quad 0 < l < L\end{aligned} \tag{3.21}$$

where $L = N/M$, with N and M being the number of total subcarriers and the number of pilot signals. Its schematic diagram of the pilot-based channel estimation with linear interpolation is shown in Fig. 3.13. It is noteworthy that this method needs lower computational complexity than those of channel estimation methods.

3.4.2 Lowpass Filtering in Transform Domain

LS-based channel estimation can achieve a better performance in a slow fading channel as long as the noise power is moderately small. However, this assumption is impractical due to the fact that a wideband radio channel is usually time-variant, frequency selective, and noisy. The pilot signals may be corrupted by ICI introduced by the fast variation of the mobile channel. In addition, the performance in channel estimation will significantly degrade because of noise. As a remedy, a novel channel estimation incorporating lowpass filtering in the transform domain, as shown in Fig. 3.14, is utilized to alleviate the effects of both ICI and noise [33]. The design involves the following procedure.

1. Rough channel response obtained by LS channel estimation

We first perform initial estimation of the channel responses at pilot locations with a simple LS method used. That is,

$$\hat{H}_{scat,ls}(k) = \frac{Y_{scat}(k)}{X_{scat}(k)} = H_{sact}(k) + \frac{N_{scat}(k)}{X_{scat}(k)}, \quad k = 0, \ldots, N_{p,scat} - 1 \tag{3.22}$$

where X_{scat} and $N_{scat} = N_{scat,noise} + N_{scat,ICI}$ denote the pilot signal and the noise component consisting of ICI and noise, respectively.

2. Noise and ICI reduction

Since the true channel response $H_{scat,ls}$ in (3.22) is slowly varying with respect to the noise component N_{scat}, the "virtual high frequency" and "virtual low frequency" regions in the transformation of the estimated channel response will be mainly contributed by the true channel response and the noise, respectively. Note that the quotation marks denote the transform domain. An example is shown in Fig. 3.15. This suggests that these two components can be successfully separated by transforming the estimated channel responses of the pilot tones into the transform domain with discrete Fourier transform (DFT) or FFT. The transformation of $\hat{H}_{scat,ls}(k)$ is given by

$$\dot{G}_{scat}(w) = \sum_{k=0}^{N_{scat}-1} \hat{H}_{scat,ls}(k) \exp\left(-j\frac{2\pi}{N_{scat}}kw\right) \tag{3.23}$$

where w is the transform domain index for $w \in [0,\ N_{p,scat} - 1]$. An ideal lowpass filter is then performed on the transformed data, leading to

$$\widehat{G}_{scat}(w)=\begin{cases}\dot{G}_{scat}(w), & 0\le w\le w_c,\ N_{p,scat}-w_c\le w\le N_{p,scat}-1\\ 0, & \text{otherwise}\end{cases} \tag{3.24}$$

where w_c is the "virtual cutoff frequency" of the filter. After filtering, noise and ICI effects can be effectively reduced.

3. Interpolation approach

Under the assumption of slow-variation, the channel transfer function can be viewed as the sum of several sinusoidal functions with respect to *k*. However, the number and the "virtual frequencies" of the sinusoids vary due to the changing in the mobile radio channel. To avoid the model mismatch problem, we do not transform $\widehat{G}_{scat}(w)$ back to frequency domain and then perform interpolation. Instead, a high-resolution interpolation approach based on zero-padding is used. First, the $N_{p,scat}$-sample transform-domain sequence $\widehat{G}_{scat}(w)$ is extended to an N_c-sample sequence $\widehat{G}(q)$ by padding with $N_c-N_{p,scat}$ zero samples at the "virtual high frequency" region as follows:

$$\widehat{G}(q)=\begin{cases}\widehat{G}_{scat}(q), & 0\le q\le w_c\\ 0, & w_c<q<N_c-w_c\\ \widehat{G}_{scat}(q-N_c+N_{p,scat}), & N_c-w_c\le q\le N_c-1\end{cases} \tag{3.25}$$

This N_c-sample sequence $\widehat{G}(q)$, in its physical meaning, is the Fourier transform of the desired estimate of the channel transfer function. By performing an N_c-point inverse DFT/FFT (IDFT/IFFT), the estimated transfer function is obtained as

$$\widehat{H}_{filter}(k)=a\sum_{q=0}^{N_c-1}\widehat{G}(q)\exp\left(j\frac{2\pi}{N_c}qk\right),\quad 0\le k\le N_c-1 \tag{3.26}$$

where *a* denotes normalized coefficient term after IDFT.

4. Dynamic selection of cutoff frequency

According to (3.24), the accuracy of the channel estimation with lowpass filtering is substantially dependent on the "virtual cutoff frequency" w_c. With a large value of w_c selected, noise and ICI effects can only be reduced slightly, while the desired signal will be suppressed with a small value of w_c used. A proper value of w_c can be determined adaptively by the ratio.

$$R = \frac{\left[\sum_{w=0}^{w_c} \left|\bar{G}_{scat}(w)\right|^2 + \sum_{w=N_{scat}-w_c}^{N_{scat}-1} \left|\bar{G}_{scat}(w)\right|^2\right]}{\sum_{w=0}^{N_{scat}-1} \left|\bar{G}_{scat}(w)\right|^2} \tag{3.27}$$

where $\bar{G}_{scat}(w)$ is the average of $\dot{G}_{scat}(w)$ of the present OFDM symbol and those of ten previous OFDM symbols. By a rule of thumb, the ratio R is selected within 0.9 and 0.95.

The channel estimator with lowpass filtering can achieve better performance in the penalty of higher computational complexity. This is because additional operations are necessary for the implementation of a lowpass filter, DFT/FFT, and IDFT/IFFT.

3.5 Computer Simulations

Computer simulations are conducted to evaluate the performance of synchronization and channel estimation in a DVB-T system. The channel model employed is given by

$$y(t) = \frac{\rho_0 x(t) + \sum_{i=1}^{K-1} \rho_i e^{-j\theta_i} x(t-\tau_i)}{\sqrt{\sum_{i=0}^{K-1} \rho_i^2}} \tag{3.28}$$

where $x(t)$ and $y(t)$ are input and output signals, K is the number of fingers set to be 20, and θ_i, ρ_i and τ_i denote the phase shift from scattering, the attenuation, and the relative delay associated with *i*th path, respectively. Note that the first term in the numerator in (3.26) represents the line of sight ray. The parameter setting of channel response is summarized in Table 3.5. In simulation, the relationship between SNR and E_b/N_0 can be defined as

$$\frac{E_b}{N_0} = \frac{\text{bit power}}{\text{noise power}} = \frac{\frac{E_b}{T_s}}{N_0 \cdot \frac{1}{T_s}} = \frac{\frac{E_s}{T_s \cdot M}}{N_0 \cdot B} = \text{SNR} \cdot \frac{1}{M} \tag{3.29}$$

When the system transmit power is normalized to one, then the noise power is given by σ^2 corresponding to a specific E_b/N_0 can be generated by

$$\sigma^2 = \frac{N_0}{E_b} \tag{3.30}$$

where E_s is the symbol energy, T_s is the symbol duration, *B* is the system bandwidth,

and M is the modulation order.

In the first simulation, the performance of synchronization is investigated in a DVB-T system. The simulation parameter setting is listed in Table 3.6. The result of cyclic-prefix-based coarse timing synchronization shown in Fig. 3.16 indicates that coarse timing synchronization may cause an error of one or two samples. Hence, a fine timing synchronization is required to enhance the performance. The result obtained by the pilot-based fine timing synchronization as shown in Fig. 3.17, demonstrates that a precise symbol timing position can be obtained.

In the second simulation, the performance of channel estimation is examined in a DVB-T system. The BER versus E_b/N_0 plots obtained by the LS channel estimation with linear interpolation and lowpass filtering in the transform domain are shown in Fig. 3.18 (a)-(b) for the mobile speed v of 0 and 20 m/s, respectively. Note that the Jake's model is used to model the fading channel. From Fig. 3.18 (a), we observe that lowpass filtering can successfully suppress the noise and provides about 1dB improvement as compared with the LS channel estimation for the BER of 6×10^{-4}. This is because that the effect of ICI is negligible for low velocity. On the contrary, in the case of high velocity, the performance of both methods is degraded due to ICI, but the lowpass filtering slightly outperforms than the LS method. These simulation results confirm that the lowpass filtering can obtain better performance than the LS channel estimation.

3.6 Summary

A standard DVB-T system is introduced. The cyclic-prefix based and pilot-based schemes are then constructed to enhance the accuracy of timing and frequency offset estimation over a fading channel. In addition, LS channel estimation with linear interpolation and lowpass filtering in the transform domain are also included for correct estimation of the channel response. A DVB-T system incorporating the previously mentioned technique proves to be robust in a typical urban environment.

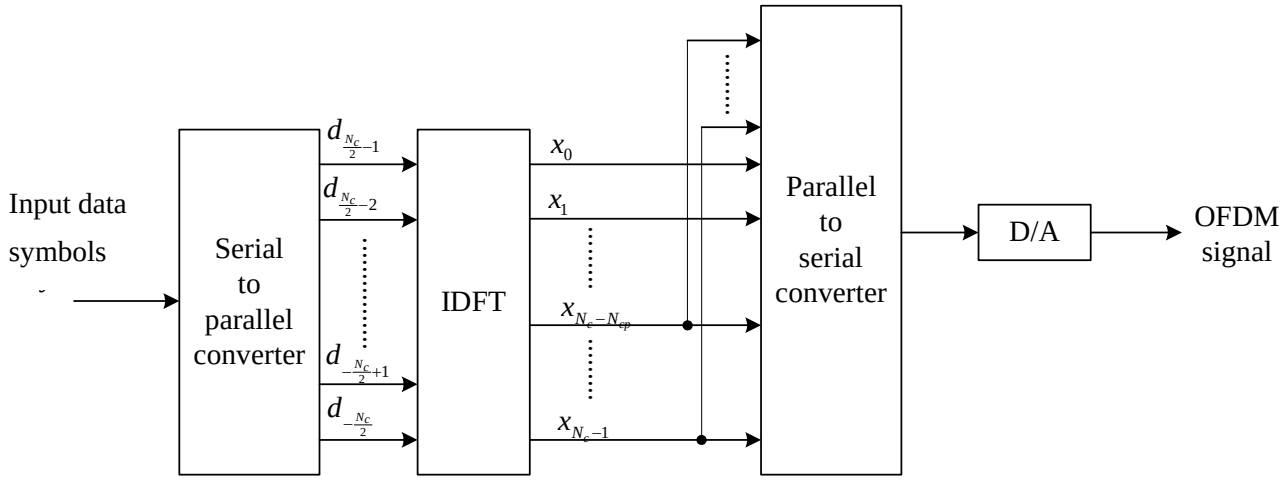

Figure 3.1: Digital implementation of appending cyclic prefix into OFDM signal in transmitter.

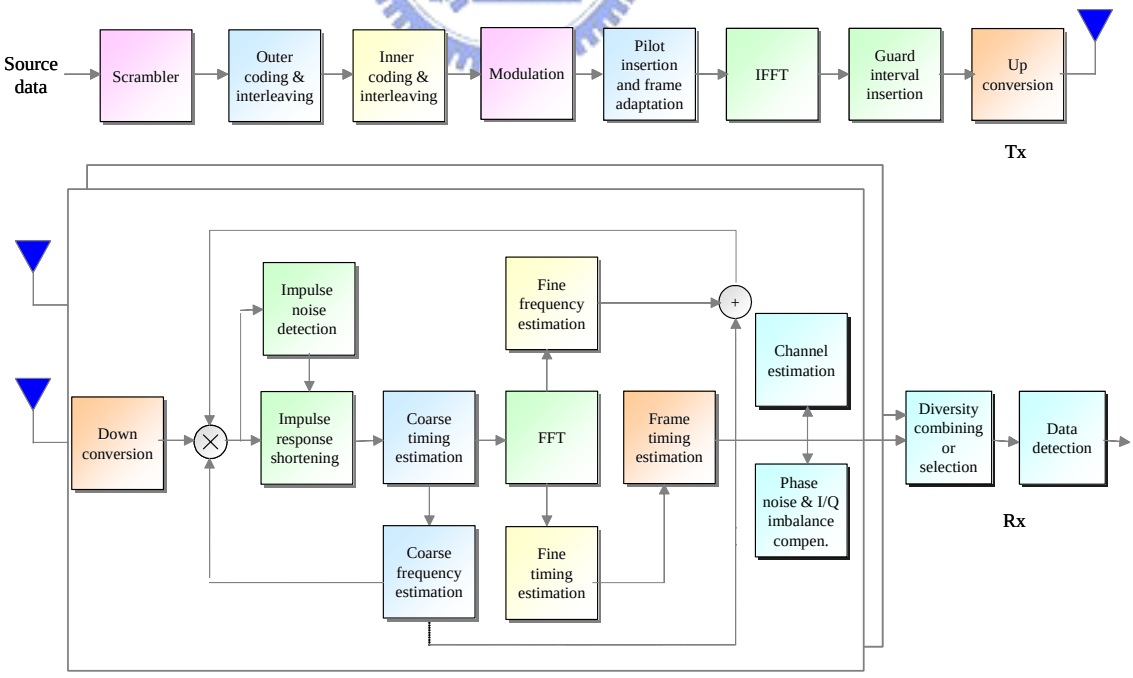

Figure 3.2: Transceiver architecture for DVB-T system.

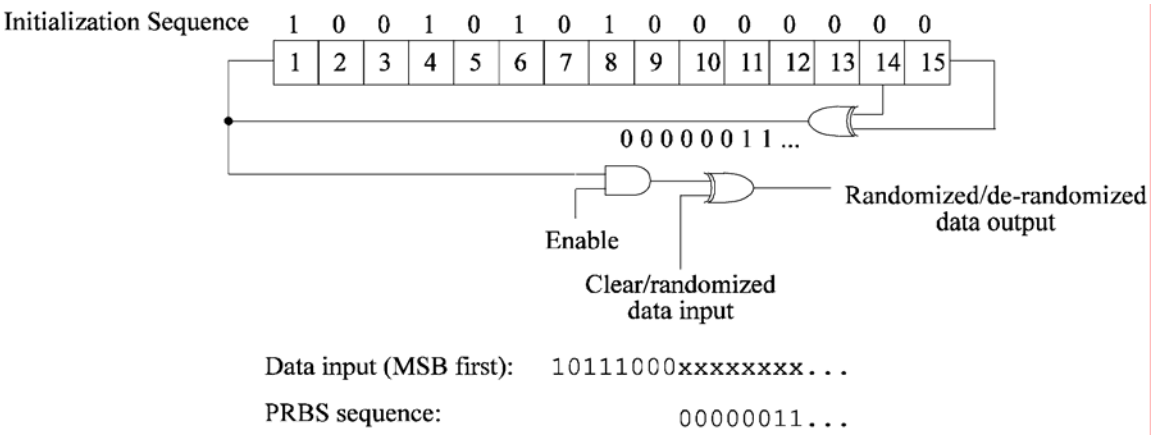

Figure 3.3: Scrambler/descrambler schematic diagram in DVB-T system.

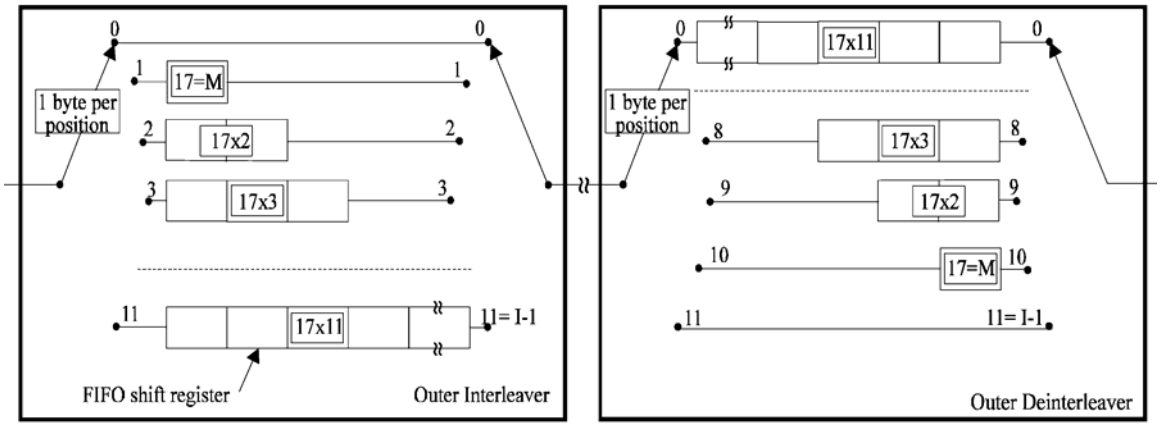

Figure 3.4: Conceptual diagram of outer interleaver and deinterleaver DVB-T system.

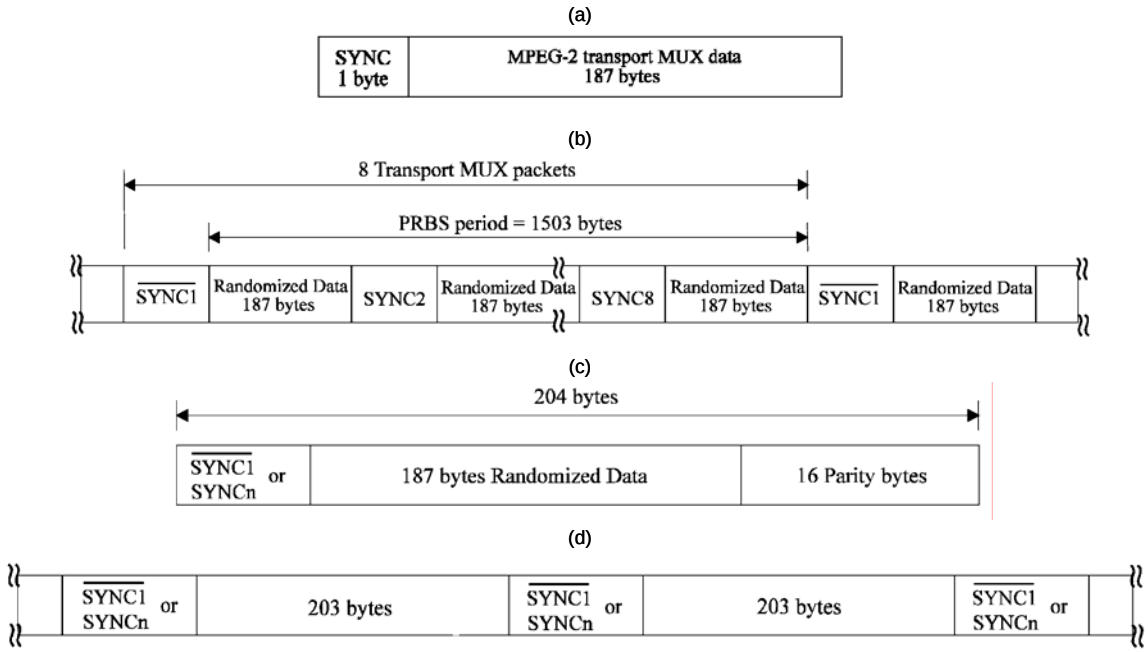

Figure 3.5: Data format of DVB-T system. (a) MPEG-2 transport MUX packet. (b) Randomized transport packets: Sync bytes and randomized data bytes. (c) RS(204, 188, 8) error protected packets. (d) Data structure after outer interleaving.

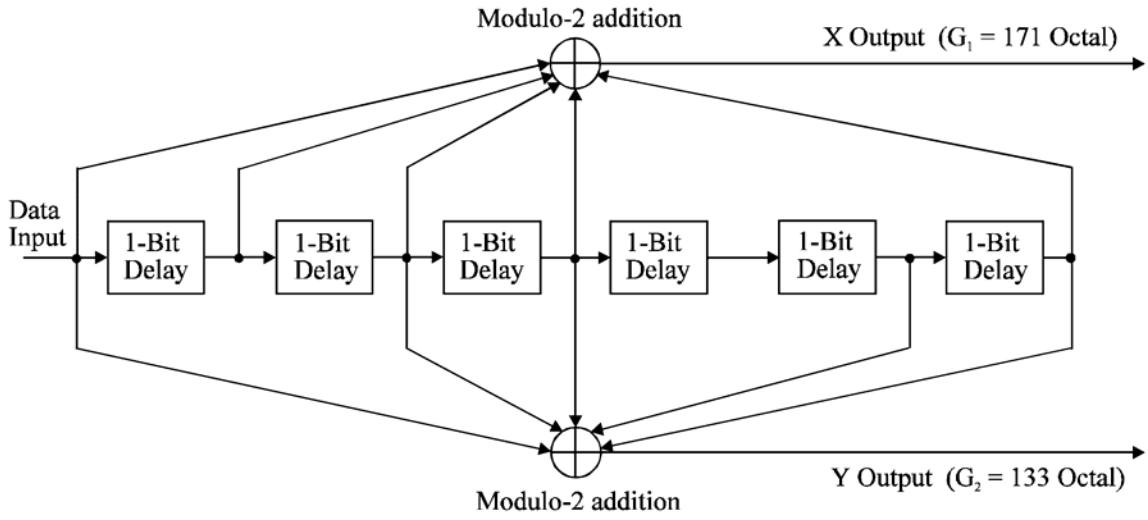

Figure 3.6: Mother convolutional code of rate 1/2 in DVB-T system.

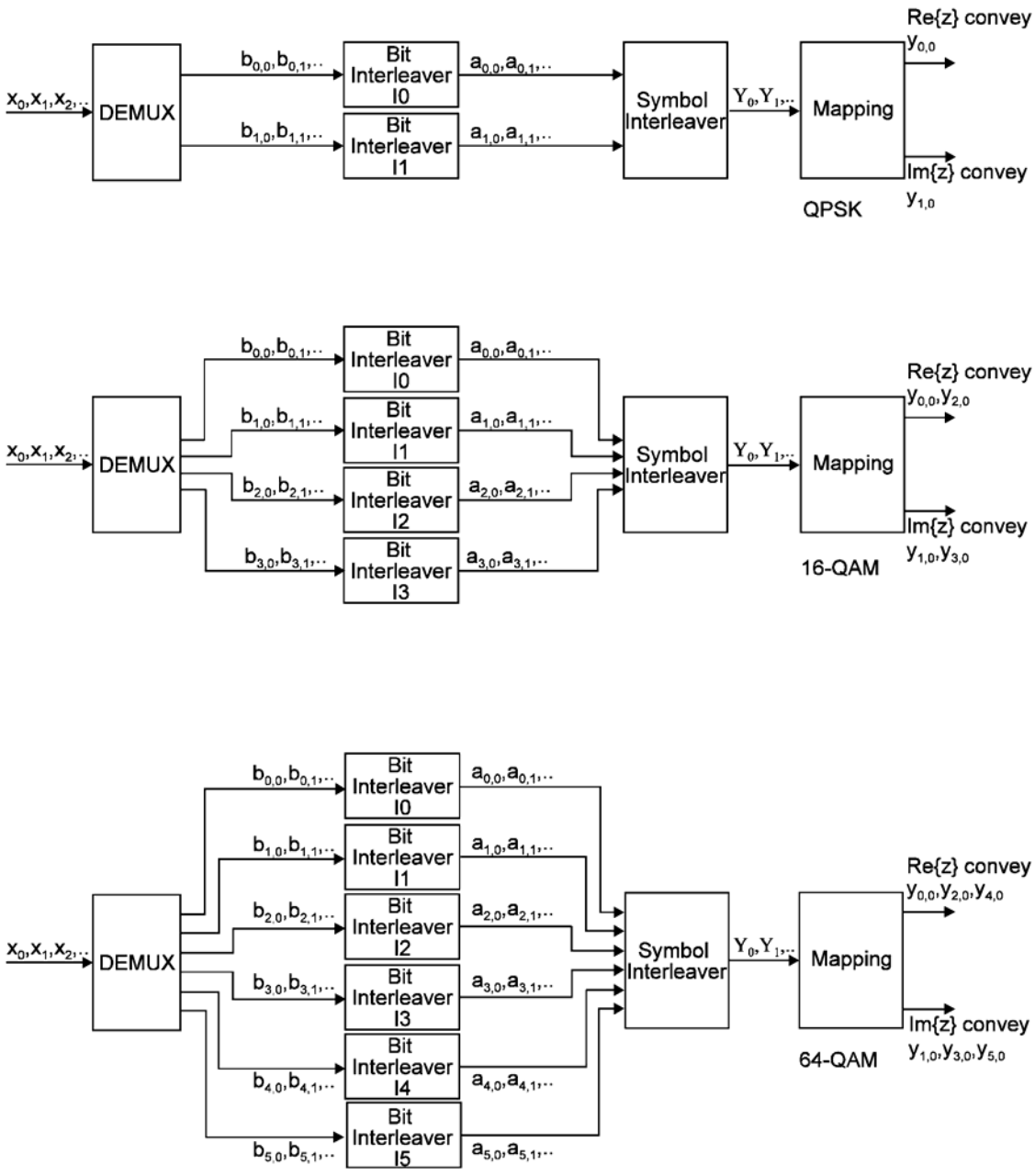

Figure 3.7: Mapping of input bits onto output modulation symbols, for non-hierarchical transmission modes in DVB-T system.

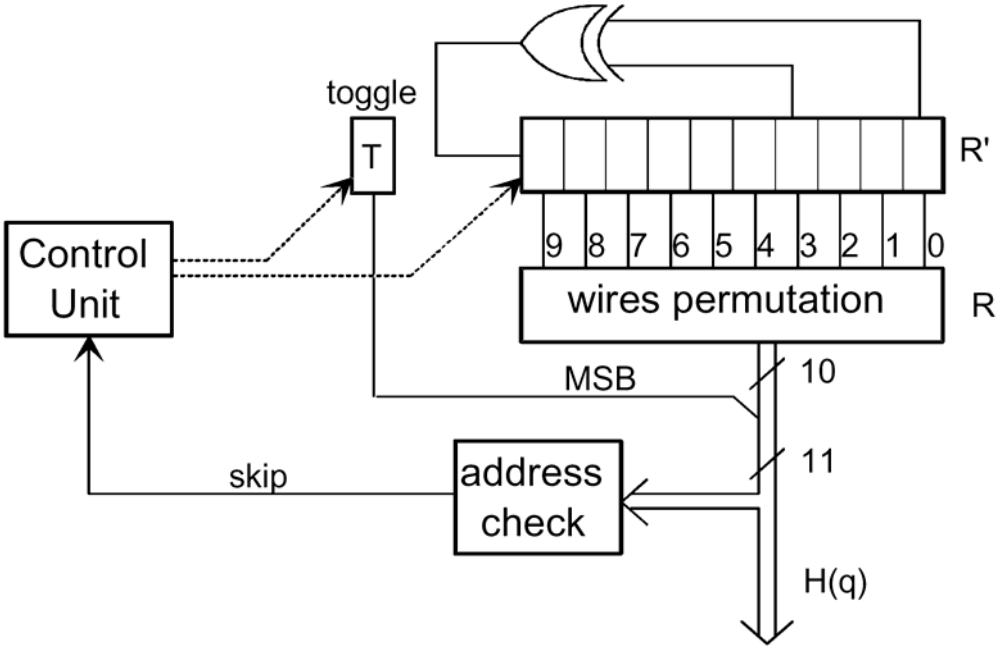

Figure 3.8: Block diagram of symbol interleaver address generation scheme for 2k mode in DVB-T system.

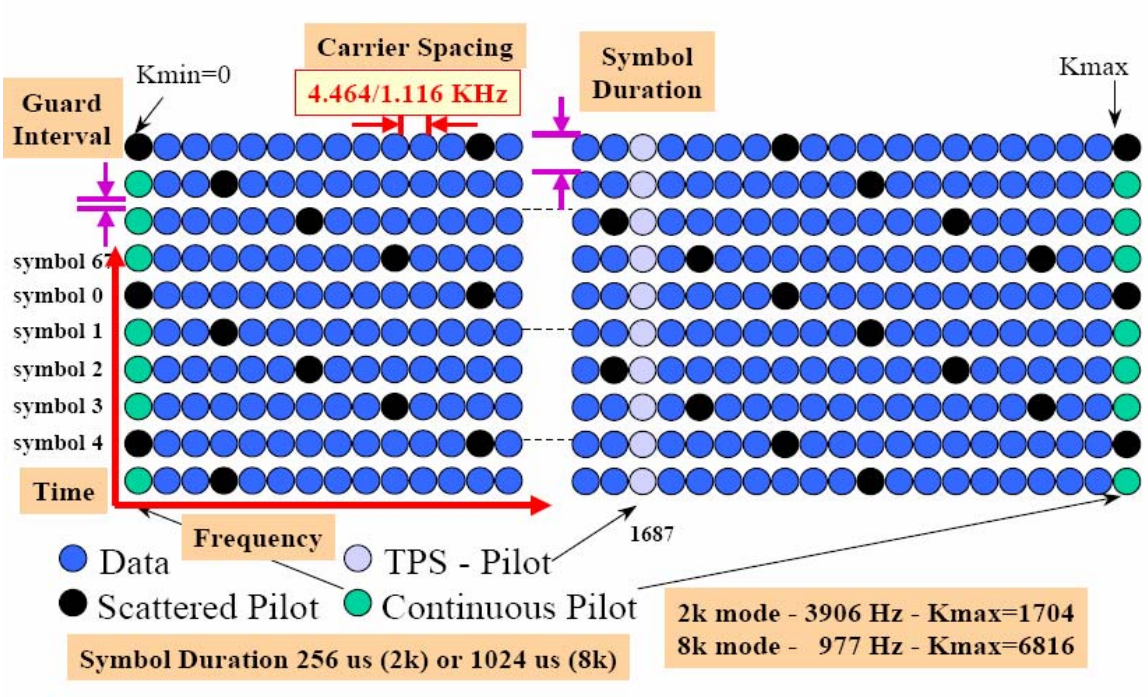

Figure 3.9: Frame structure in DVB-T system.

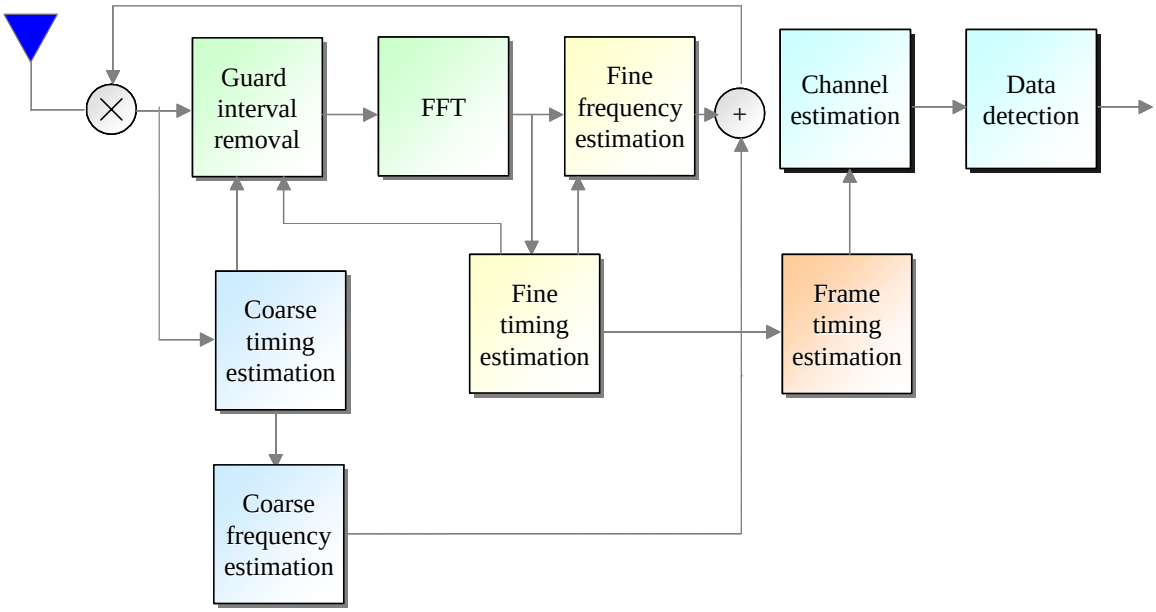

Figure 3.10: Block diagram of synchronization and channel estimation in DVB-T system.

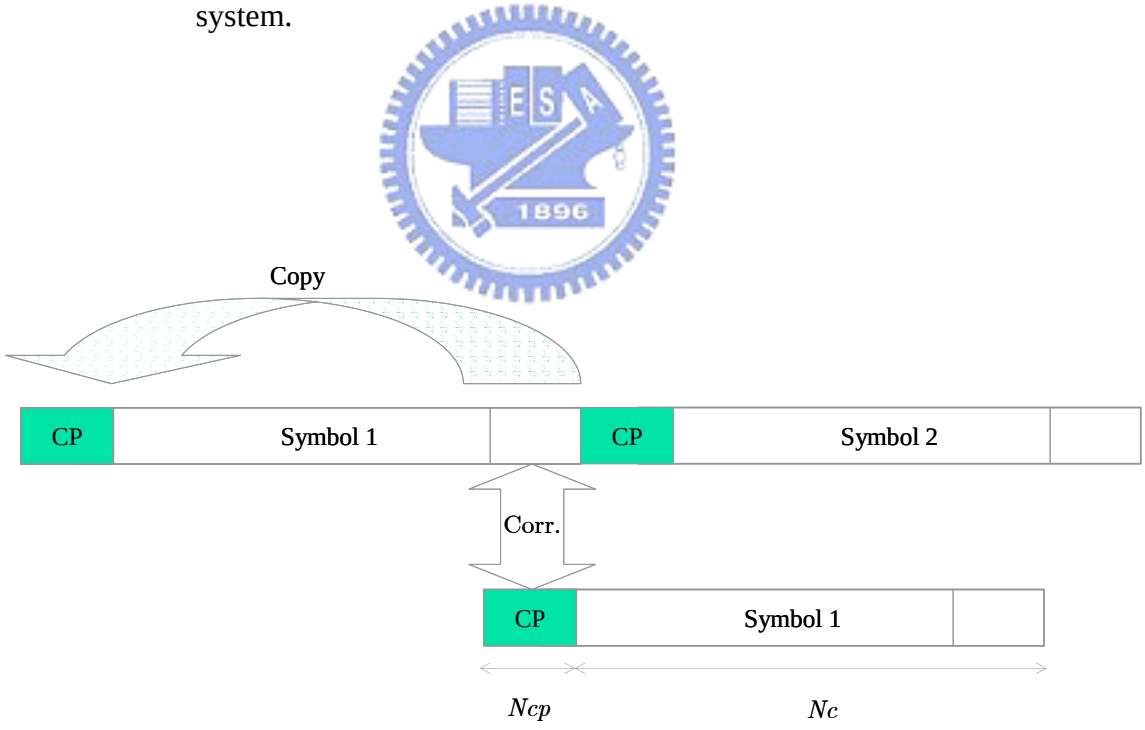

Figure 3.11: Illustration of OFDM signal with cyclic prefix for coarse timing and frequency offset synchronization.

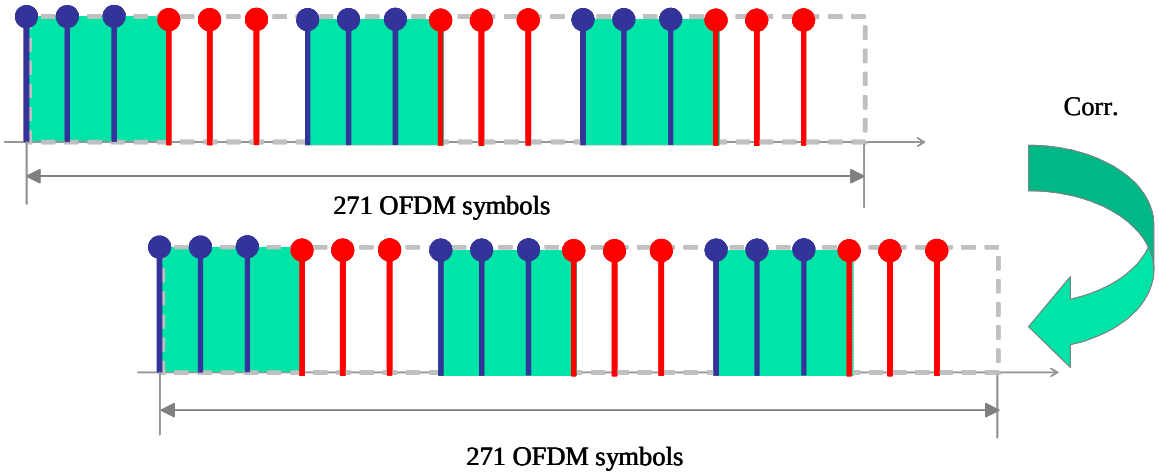

Figure 3.12: Illustration of pilot-based correlation for fine frequency synchronization in synchronization and channel estimation in DVB-T system.

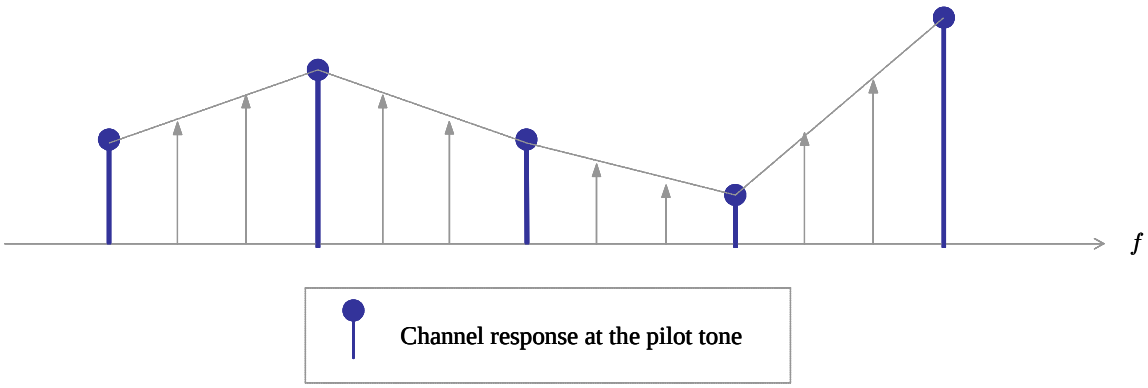

Figure 3.13: Illustration of pilot-based channel estimation with linear interpolation in DVB-T system.

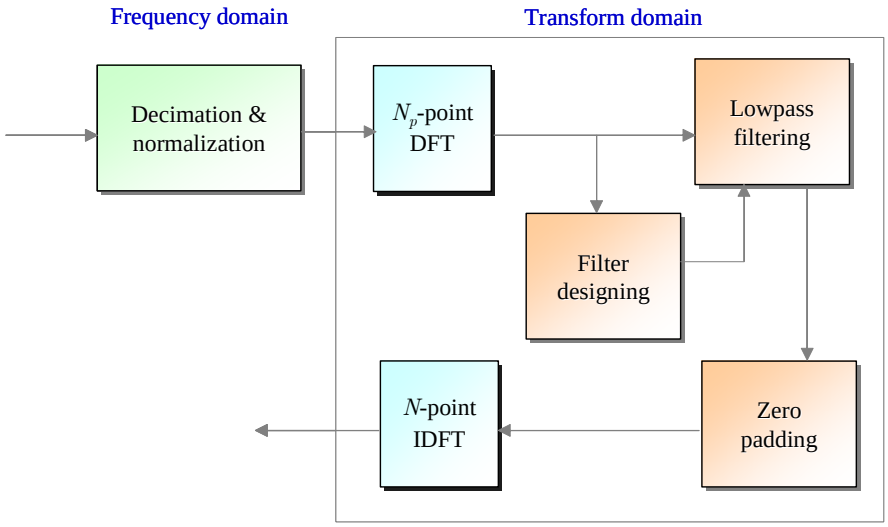

Figure 3.14: Block diagram of channel estimation with lowpass filtering in transform domain in OFDM system.

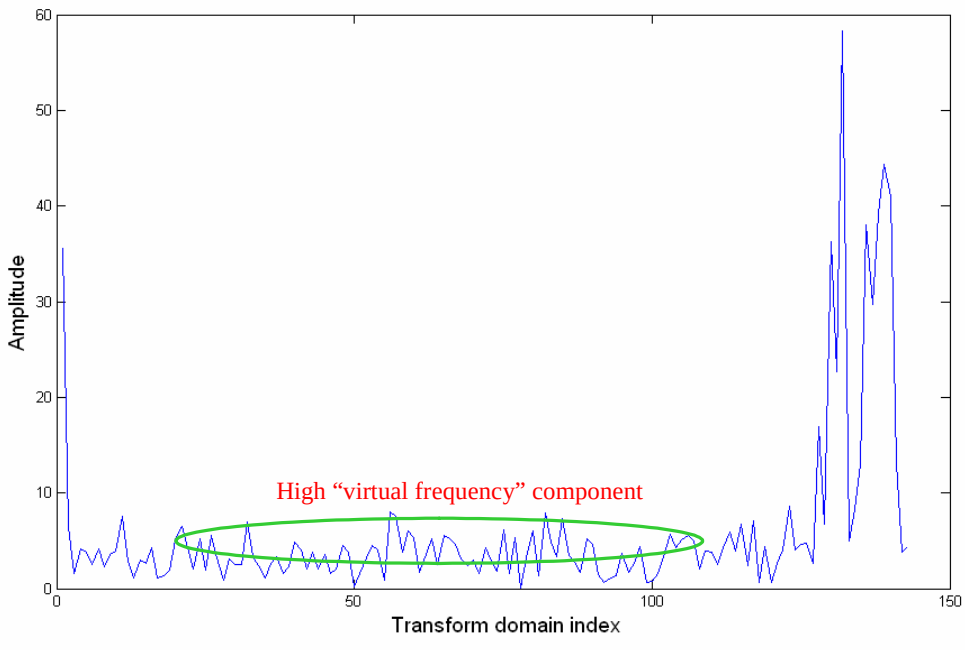

Figure 3.15: Estimated channel amplitude responses in transform domain of OFDM system.

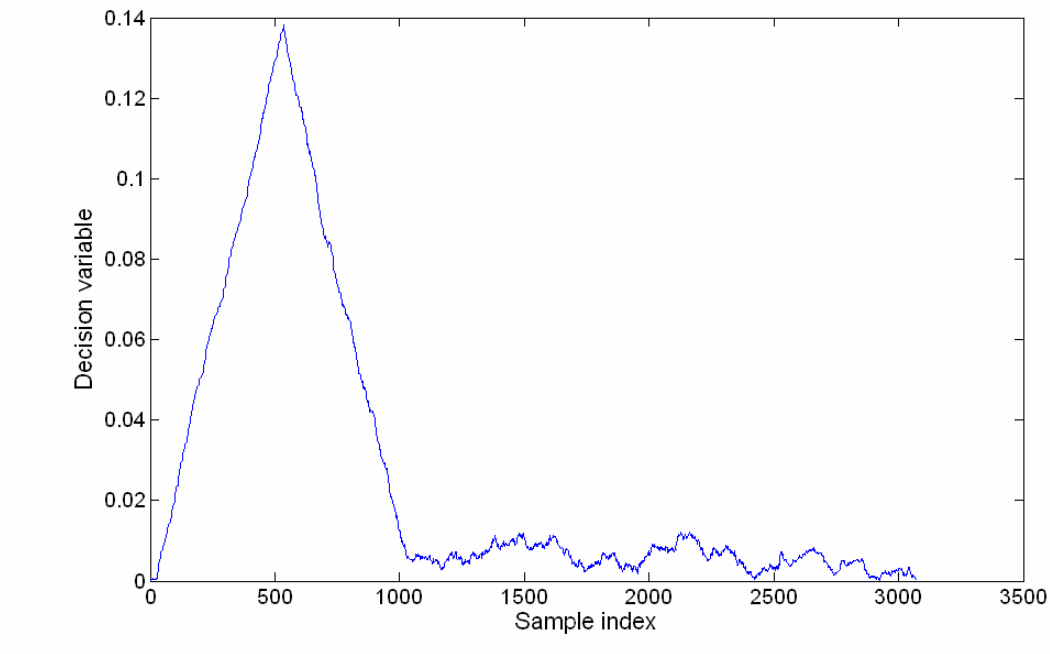

Figure 3.16: Decision variable versus sample index with coarse timing synchronization in DVB-T system.

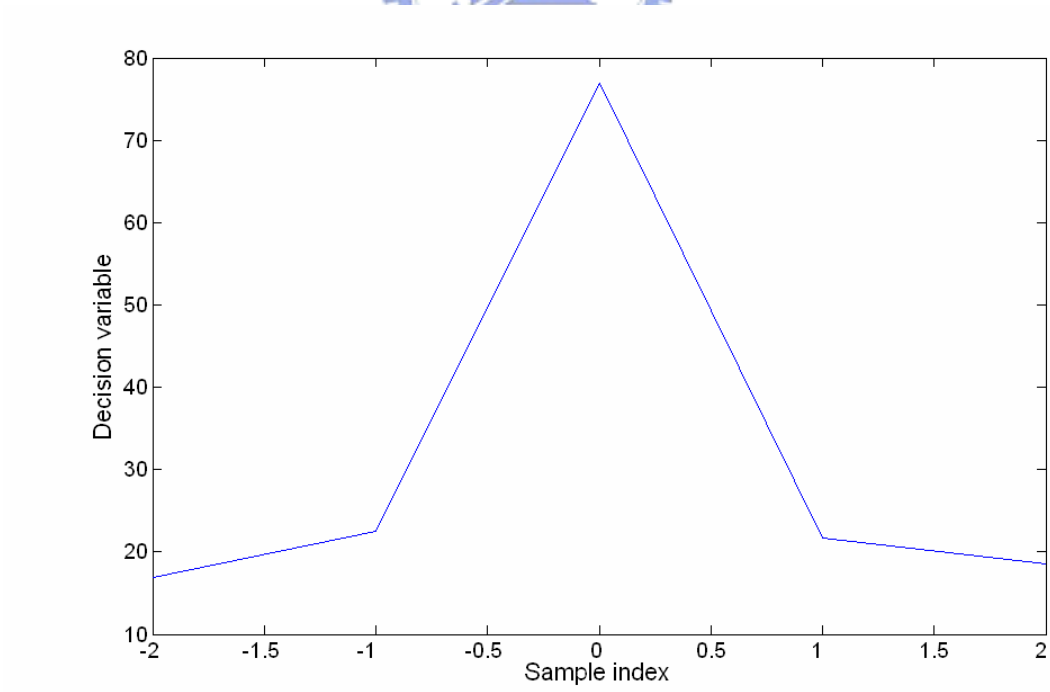

Figure 3.17: Decision variable versus sample index with fine timing synchronization in DVB-T system.

(a)

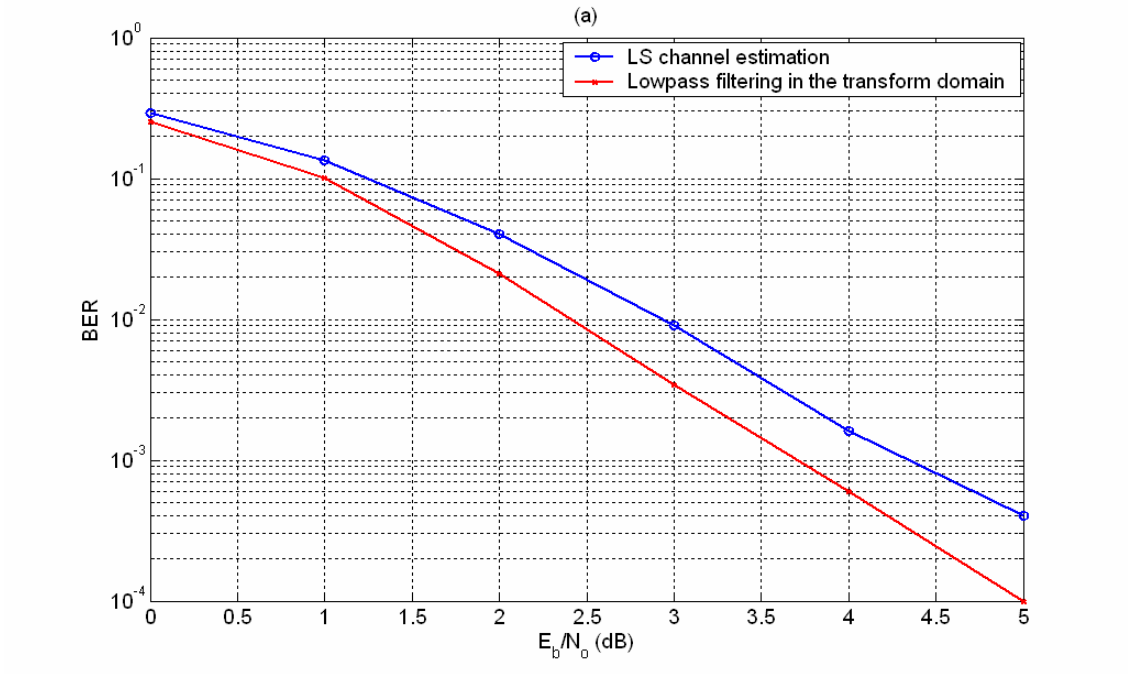

(b)

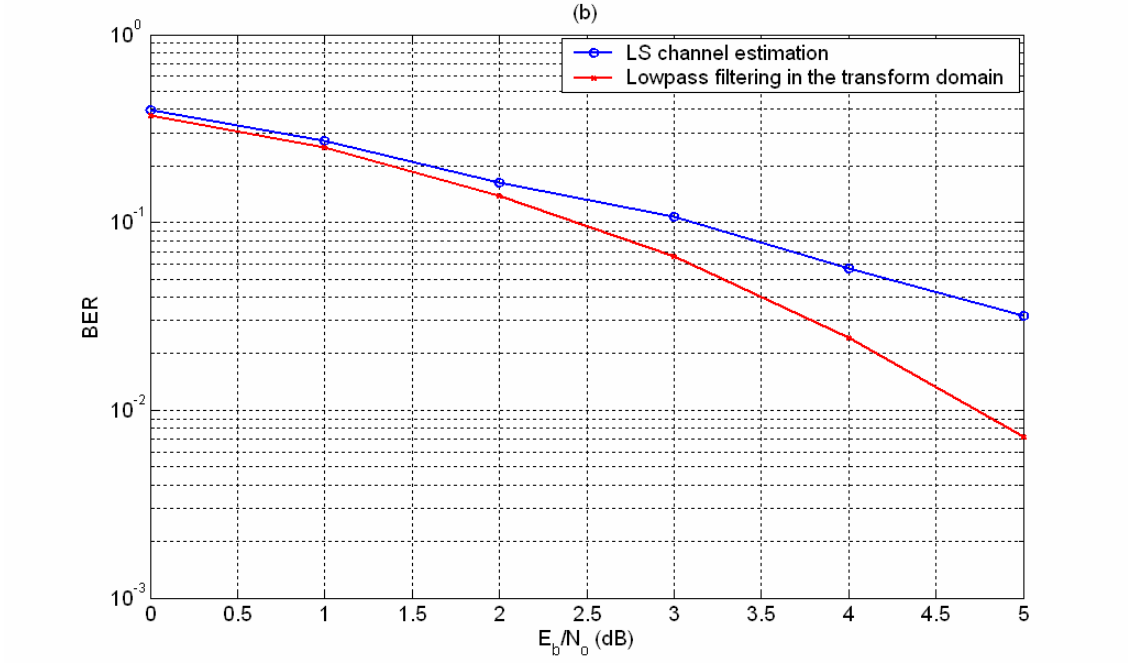

Figure 3.18: BER performances versus E_b/N_0 of channel estimation methods in DVB-T system with mobile speed *v* of (a) 0 m/s. (b) 20 m/s.

Table 3.1: Bit permutations for (a) 2k mode (b) 8k mode in OFDM-based DVB system.

(a)

R'_i bit positions	9	8	7	6	5	4	3	2	1	0
R_i bit positions	0	7	5	1	8	2	6	9	3	4

(b)

R'_i bit positions	11	10	9	8	7	6	5	4	3	2	1	0
R_i bit positions	5	11	3	0	10	8	6	9	2	4	1	7

Table 3.2: Signal constellation and mapping in DVB-T system. (a) Constellation points are $z \in \{n + jm\}$ with values of n, m. (b) Normalization factors for data symbols.

(a)

Modulation scheme	n	m
QPSK	-1, 1	-1, 1
16QAM with $\alpha = 1$	-3, -1, 1, 3	-3, -1, 1, 3
16QAM with $\alpha = 2$	-4, -2, 2, 4	-4, -2, 2, 4
16QAM with $\alpha = 4$	-6, -4, 4, 6	-6, -4, 4, 6
64QAM with $\alpha = 1$	-7, -5, -3, -1, 1 , 3, 5, 7	-7, -5, -3, -1, 1 , 3, 5, 7
64QAM with $\alpha = 2$	-8, -6, -4, -2, 2, 4, 6 ,8	-8, -6, -4, -2, 2, 4, 6 ,8
64QAM with $\alpha = 4$	-10, -8, -6, -4, 4, 6 ,8, 10	-10, -8, -6, -4, 4, 6 ,8, 10

(b)

Modulation scheme	Normalization factor
QPSK	$K_{MOD} = z/\sqrt{2}$
16QAM with $\alpha = 1$	$K_{MOD} = z/\sqrt{10}$
16QAM with $\alpha = 2$	$K_{MOD} = z/\sqrt{20}$
16QAM with $\alpha = 4$	$K_{MOD} = z/\sqrt{52}$
64QAM with $\alpha = 1$	$K_{MOD} = z/\sqrt{42}$
64QAM with $\alpha = 2$	$K_{MOD} = z/\sqrt{60}$
64QAM with $\alpha = 4$	$K_{MOD} = z/\sqrt{108}$

Table 3.3: Numerical values for OFDM parameters in 8k and 2k modes of 8MHz channel in DVB-T system.

Parameter	8K mode	2K mode
Number of carrier K	6817	1705
Value of carrier number $K_{\min}$	0	0
Value of carrier number $K_{\max}$	6816	1704
Duration T_u	896 μs	224 μs
Carrier spacing $1/T_u$	*1116 Hz*	*4464 Hz*
Spacing between carriers $K_{\min}$ and $K_{\max}$ $(K-1)/T_u$	*7.61 MHz*	*7.61 MHz*
Note1: Values in italics are approximate values		

Table 3.4: Required C/N for non-hierarchical transmission to achieve a $\text{BER} = 2\times10^{-4}$ after the Viterbi decoder for all combinations of coding rates and modulation types in DVB-T system.

Modulation	Code rate	Gaussian channel	Ricean channel	Rayleigh channel
QPSK	1/2	3.1	3.6	5.4
	2/3	4.9	5.7	8.4
	3/4	5.9	6.8	10.7
	5/6	6.9	8.0	13.1
	7/8	7.7	8.7	16.3
16QAM	1/2	8.8	9.6	11.2
	2/3	11.1	11.6	14.2
	3/4	12.5	13.0	16.7
	5/6	13.5	14.4	19.3
	7/8	13.9	15.0	22.8
64QAM	1/2	14.4	14.7	16.0
	2/3	16.5	17.1	19.3
	3/4	15.0	18.6	21.7
	5/6	19.3	20.0	25.3
	7/8	20.1	21.0	27.9

Table 3.5: Relative power, phase and delay values for standard channel model of DVB-T system.

i	ρ_i	τ_i [μs]	θ_i [rad]
1	0.057662	1.003019	4.855121
2	0.176809	5.422091	3.419109
3	0.407163	0.518650	5.864470
4	0.303585	2.751772	2.215894
5	0.258782	0.602895	3.758058
6	0.061831	1.016585	5.430202
7	0.150340	0.143556	3.952093
8	0.051534	0.153832	1.093586
9	0.185074	3.324866	5.775198
10	0.400967	1.935570	0.154459
11	0.295723	0.429948	5.928383
12	0.350825	3.228872	3.053023
13	0.262909	0.848831	0.628578
14	0.225894	0.073883	2.128544
15	0.170996	0.203952	1.099463
16	0.149723	0.194207	3.462951
17	0.240140	0.924450	3.664773
18	0.116587	1.381320	2.833799
19	0.221155	0.640512	3.334290
20	0.259730	1.368671	0.393889

Table 3.6: Simulation parameters of DVB-T system.

Number of transmit/receive antenna	1/1
Data rate	4.98 Mbps
Modulation	QPSK
Coding rate	1/2
Symbol time	280 μs
Guard time	56 μs
Subcarrier spacing	4.464 KHz
FFT length	2048
System clock	64/7 MHz
OFDM symbols	272 symbols (4 frames/per superframe)
Carrier frequency	474 MHz

Chapter 4

Diversity Reception and Phase Noise Compensation in DVB-T Systems

As mentioned in Section 2.1, diversity is effective to combat detrimental effects in wireless fading channels because the probability of two or more independent faded channels in a deep fade simultaneously is small. On the other hand, oscillator phase noise is a potentially serious problem because of the common necessity to employ relatively low cost tuners in the receivers. It affects communication systems in two ways: CPE and ICI (referred to Section 2.2). We propose some solutions to combat against these effects. They are MRC, low-pass filtering in the transfer domain, and decision feedback phase noise compensator with batch processing. The details will be discussed in sections to come.

4.1 Diversity Reception at Different Stages in DVB-T Systems

We will focus on space diversity reception in this chapter. Space diversity is also known as antenna diversity. In practice, we consider dual receive antennas employed in a DVB-T system. Dual antennas separated physically by a distance can guarantee that the transmitted signals from different antennas go through low correlated fading paths. This kind of diversity scheme is widely used due to simplicity and low-cost. Furthermore, it requires no extra frequency spectrum. Space diversity can be divided into two categories: selective and combining diversity schemes. A more robust reception is achieved when using more than one receive antenna by combining or

selecting the signals from different branches. The improved reception can be used to increase the transmission reliability for both portable and mobile television receivers, such as those found in cars. Selective diversity is to select the strongest signal among diversity branches, which is easy for implementation. On the other hand, combining diversity combines signals from different branches to get better performance. The trade-off between BER performance and computational complexity determines which diversity scheme is used. In Fig. 4.1, we use various diversity reception schemes at different stages in a DVB-T system. The discussed diversity reception schemes include MRC, symbol-based selective diversity (SBSD), cyclic delay diversity (CDD), MRC with CDD, in-/post-Viterbi selective diversity (IVSD/PVSD), and packet-based selective diversity (PBSD). For convenience, we assume perfect synchronization and perfect channel estimation. These schemes are described as follows.

4.1.1 Maximal Ratio Combining

In the MRC scheme, the outputs of the dual receive antennas are linearly combined so as to maximize the instantaneous SNR. The coefficients that yield the maximum SNR can be found from the optimization theory in Chapter 2. They are the complex conjugate of the channel responses. The algorithm in the frequency domain is given by

$$\begin{aligned} Y^{(1)} &= H^{(1)}X + N^{(1)} \\ Y^{(2)} &= H^{(2)}X + N^{(2)} \\ H^{(1)*}Y^{(1)} + H^{(2)*}Y^{(2)} &= \left(\underbrace{\left|H^{(1)}\right|^2 + \left|H^{(2)}\right|^2}_{\text{full diversity gain}} \right) X + \tilde{N} \end{aligned} \tag{4.1}$$

where the superscript denotes the antenna index. From (4.1), we can observe that “full diversity” gain is exploited. Therefore, MRC can get better performance. In an OFDM-based DVB system, each tone needs its own one-tap equalizer for channel compensation. Therefore, MRC needs twice the number of multipliers for channel compensation with single antenna. After introducing the principle and hardware cost of MRC, we compare other diversity schemes with MRC in the following sections.

4.1.2 Symbol-Based Selective Diversity

The average power p_j of the OFDM symbol in the jth branch is estimated by the receiver [1]. This estimation is done for each branch, i.e. j = 1, 2. The branch $\hat{j}$ with larger power will be selected

$$\hat{j} = \arg\max_{j} p_j \tag{4.2}$$

In SBSD, we assume that the signal power and noise power are the same in different branches. Only the channel responses are different in different branches. Moreover, channel responses don't change significantly in the frequency domain. Therefore, the scheme can suppress deep fading phenomenon by selecting larger symbol power which doesn't need channel information. As mentioned before, the channel information must be obtained in frequency domain for a DVB-T system. Therefore, SBSD can be proposed to operate before FFT. Fig. 4.1 shows that a receiver using SBSD obtains the same computational complexity as the single antenna case after FFT. Thus, SBSD would need lower computational complexity.

4.1.3 Cyclic delay Diversity

Before referring to CDD, we introduce delay diversity (DD) and phase diversity (PD) whose concepts are similar to that of CDD [2]-[5]. Usually, DD and PD are applied at multiple-antenna transmitter side.

Delay Diversity

In DD, the transmitted multi-carrier modulated signal differs only with the specific delay δ_m at the mth antenna, where m = 0,…, M-1. The block diagram of an OFDM system with the spatial transmit diversity applying DD is shown in Fig. 4.2. In order to achieve constructive and destructive superposition of the signals, the delay δ_{m} has to fulfill the condition

$$\delta_m \geq \frac{1}{B}, \qquad \forall m \tag{4.3}$$

where B is the channel coherence bandwidth. Therefore, frequency selectivity is

generated, and long burst errors induced from deep flat fading are avoidable. Fig. 4.3 shows the effect of DD over a typical indoor channel. But the disadvantage of DD is that the additional delays increase the total delay spread at the receiver antenna, i.e. the effective cyclic prefix length is reduced relatively. To overcome this issue, phase diversity scheme is presented.

Phase Diversity

In PD, the transmitted multi-carrier modulated signal differs only with the specific phase offset. The block diagram of an OFDM system with the spatial transmit diversity applying PD is shown in Fig. 4.4. In order to achieve constructive and destructive superposition of the signals, the phase offset $\Phi_{m,k}$ has to fulfill the condition

$$\Phi_{m,k} \geq 2\pi f_k \frac{1}{B}, \qquad \forall m,\ \forall n \tag{4.4}$$

where $f_k = k/T_s$ is the kth tone frequency, and T_s is the OFDM symbol duration without the cyclic prefix. Therefore, frequency selectivity is generated. But the disadvantage of PD is that the scheme operates in the frequency domain, which needs the M OFDM modulation blocks. To prevent additional hardware induced from PD and the effective cyclic prefix length from being shortened by DD, the CDD is exploited in place of PD and DD.

Cyclic Delay Diversity

In CDD, the signal is not truly delayed but cyclically shifted. The basic idea behind the new scheme is to convert time-selectivity of the channel into frequency-selectivity so that channel coding which is applied mainly in frequency domain in the DVB-T system is more effective. The equivalence between PD and CDD is a property of DFT and can directly be seen from the length N_c IDFT definition

$$\begin{aligned} x(l) &= \sum_{k=0}^{N_c-1} X(k) e^{j\frac{2\pi}{N_c}kl} \\ \underbrace{x((l-\delta_{cy}) \bmod N_c)}_{\text{CDD signal}} &= \sum_{k=0}^{N_c-1} \underbrace{e^{-j\frac{2\pi}{N_c}k\delta_{cy}} X(k)}_{\text{PD signal}} e^{j\frac{2\pi}{N_c}kl} \end{aligned} \tag{4.5}$$

where l, k, $x(l)$, and $X(k)$ denote the discrete time, frequency, and the

complex-valued signals in time and frequency domain respectively with *l*, *k*. δ_{cy} stands for cyclic time shift. From (4.5), the operation for PD has to be done before the OFDM modulation. So for an *M*-antennas system with PD, the *M* OFDM modulation blocks have to be constructed. On the other hand, only one OFDM block is required in CDD. Thus the implementation of CDD is more efficient, and has the same functionality as those of DD/PD. However, all schemes of DD, PD and CDD are often applied in the transmitter. To implement them in the receiver side, we derive the equivalence between the transmitter and receiver with CDD. The received signals with CDD applied at the transmitter side can be written as

$$\begin{aligned} &\text{Rx1: } y^{(1)}(t) = h^{(1)}(t) * x(t) + n^{(1)}(t) \\ &\text{Rx2: } y^{(2)}(t) = h^{(2)}(t-\delta_{cy}) * x(t-\delta_{cy}) + n^{(2)}(t-\delta_{cy}) = y^{(1)}(t-\delta_{cy}) \end{aligned} \tag{4.6a}$$

And the received signals with CDD applied at the receiver side can be written as

$$\begin{aligned} &\text{Rx1: } r^{(1)}(t) = h^{(1)}(t) * x(t) + n^{(1)}(t) \\ &\text{Rx2: } r^{(2)}(t) = r^{(1)}(t-\delta_{cy}) = h^{(2)}(t-\delta_{cy}) * x(t-\delta_{cy}) + n^{(2)}(t-\delta_{cy}) \end{aligned} \tag{4.6b}$$

where Rx denotes the receive antenna. From (4.6a) and (4.6b), the equivalence is mainly based on the linear characteristics of convolution and delay. Fig. 4.5 shows the equivalence model of the transmitter and receiver using CDD. Thus, CDD can be applied in the receiver. From Fig. 4.5, we know that the implementation of CDD only needs an adder and a man-made cyclic delay. The receiver structure remains unchanged compared with the single antenna case after FFT. In addition to lower computational complexity, CDD can also incorporate other diversity schemes if hardware loading can be increased. Finally, we summarize CDD as follows:

(1) Standard compatibility, i.e. CDD can be applied without changing the transmitter.
(2) No necessity of the multiple channel estimators; therefore lower the receiver complexity.
(3) The number of receive antennas is arbitrary.
(4) Low implementation complexity, due to the simple cyclic shifts in the time domain.
(5) CDD can incorporate other diversity schemes to enhance the system performance.

Maximal Ratio Combining with Cyclic Delay Diversity

As discussed above, it is easy to combine CDD with other diversity reception schemes [5], e.g. MRC with CDD, as shown in Fig 4.6. Fig. 4.7 shows the BER performances of MRC, CDD, and MRC with CDD in a DVB-T system with cyclic delay varied as a parameter. We observe that the value of cyclic delay is important, which should be larger than RMS delay spread of a channel model. The RMS delay spread of Rayleigh fading channel model in a DVB-T system is about 1.2689 μs (see Section 4.3). Therefore, the system with the cyclic delay $\delta_{cy} = 1.8$ μs gets better performance. On the other hand, MRC with CDD outperforms conventional MRC. This is because MRC with CDD not only gets full diversity gain, but also rejects long burst errors.

4.1.4 In-Viterbi Selective Diversity

In wireless communication, channel fading and random noise effects make points on the constellation shift and thus cause decision errors. In Fig.4.8, we can know that the probability of the effects making signals of different branches shift toward error areas simultaneously is small. Therefore, we exploit the diversity scheme to increase freedom of add-compare-select (ACS) in Viterbi to help suppress the deep fading and random noise effects as shown in Fig.4.9 [6]-[7]. By the Viterbi algorithm, the branch metrics associated with the state transitions are computed and then added to the previous path metrics. The contending path metrics are compared and the path with the largest metrics is as the survivor. With the aid of diversity scheme, the path metrics are computed for each diversity branch, and then compared to select the survivor and the criterion is given by

$$\hat{j} = \arg\min_{j} d_j \tag{4.7}$$

where d_j denotes the Euclidian distance at the *j*th diversity path. Moreover, IVSD incorporating interleaver can achieve better performance. This is because interleaver combating deep fading helps IVSD more concentrate on random noise. Therefore, IVSD can suppress deep fading and random noise effects effectively.

4.1.5 Post-Viterbi Selective Diversity

In PVSD, outputs from the two Viterbi decoders are compared and selected based on path metrics [6]-[7], which is similar as IVSD. The selection strategy is also given by the (4.7). There is a main difference between IVSD and PVSD. IVSD is more instantaneous than PVSD. In other words, IVSD selects the optimum survivor state by state and PVSD selects the optimum survivor section by section. In PVSD, each received branch sequence is individually compared and selected after passing through a long path as shown in Fig 4.10.

4.1.6 Packet-Based Selective Diversity

The selection strategy of PBSD is based on the number of errors from the two RS decoders [1]. Let us assume that the number of errors in one packet of each diversity branch is given by e_1, e_2. The packet selection criterion is given by

$$\hat{j} = \arg\min_{j} e_j \tag{4.8}$$

Because the scheme will select the best syndrome, all effects are eliminated to be best of its capacity where RS decoder can correct 8 errors of one packet in a DVB-T system. Furthermore, there are three possible cases. First, received packets in two branches are equal or less than 8 errors. Second, received packets in two branches are more than 8 errors. Third, received packet in one branch is equal or less than 8 errors and that in the other branch is more than 8 errors. In consequence, in the first case, since either packet is error-free, whether we use PBSD or not doesn't make any difference. In the second case, since errors in the two packets exceed what RS decoder can tolerate, again whether we use PBSD or not doesn't make any difference. In the third case, the error-free packet will be the desired one by RS decoder and PBSD will achieve its diversity efficacy. Moreover, when SNR is higher, the random noise effect becomes smaller and other effects, e.g. ICI can be eliminated effectively. Because RS decoder is located at the end of the receiver, a receiver using PBSD will actually consist of the multiple single antenna receivers as shown in Fig. 4.1. Therefore, PBSD needs higher computational complexity than other diversity reception schemes.

4.2 Comparison of Performance and Complexity for Diversity Reception

In principle, the diversity process at the front stage needs less computational complexity. Hardware loading at the posterior stage of SBSD and CDD is the same as that of the single receive antenna. In particular, CDD only requires extra one adder, one man-made cyclic delay, and two radio frequency (RF) components, compared to the original single antenna receiver.

On the other hand, performance comparisons between each diversity scheme are illustrated in Figs. 4.7, 4.11-4.12. There are some superior schemes worth noticing. For instance, MRC implemented after the channel estimator exploits the channel information and thus provides full diversity gain. Moreover, MRC with CDD results in better performance than MRC because the effect of CDD avoids long burst error induced from deep flat fading. Another superior scheme is IVSD incorporating the interleaver, it can combat against the effects of deep fading and random noise effectively.

In summary, we list the complexity and performance comparisons between each diversity scheme as follows:

Complexity: PVSD > IVSD > MRC with CDD > MRC > SBSD > CDD

Performance: MRC with CDD > MRC > IVSD > PVSD > SBSD ≈ CDD

4.3 Phase Noise Compensation

The undesirable frequency drift introduced by the local oscillator at the receiver, which is usually called as carrier phase noise, will significantly affect an OFDM signal. As a remedy, the phase noise compensation scheme is used for enhancement of robustness against phase noise and improvement of system performance. Phase noise basically leads to the detrimental effects CPE and ICI. The effect of CPE will make received modulation symbols rotate the same angle in one OFDM symbol, as shown in Fig 4.13, and this can be successfully corrected by the channel estimation method incorporating pilot tones in DVB-T systems. However, since ICI is often regarded as the random noise effects, it cannot completely be removed in OFDM communication systems, leading to BER floor under high SNR.

In addition, Doppler shift introduced by the moving receiver terminal will cause CPE, frequency offset and ICI effects. Again, CPE can be effectively eliminated by using pilot tones. The synchronization methods can mitigate frequency offset. Finally, ICI induced by phase noise or Doppler shift can be suppressed by diversity reception using MRC, channel estimation using lowpass filtering in the transfer domain, or decision feedback phase noise compensator with batch processing. In this section, we will focus on suppression of ICI effect.

4.3.1 ICI Compensation Using MRC

Scenario considered herein involves a dual-antenna system. The received data of the ith antenna obtained by a certain sampling instant is given by

$$y_n^{(i)} = [x_n * h_n^{(i)}]\lambda_n^{(i)} + v_n^{(i)} \qquad \forall i = 1,2 \tag{4.9}$$

where $\lambda_n = e^{j\phi(n)}$ and $v_n^{(i)}$ denote phase noise and AWGN of power σ_v^2, respectively [20]. After N_c-FFT processing, the received signal in the frequency domain can be expressed as

$$Y_k^{(i)} = (1/N_c)X_k H_k^{(i)} \Lambda_0^{(i)} + \underbrace{1/N_c \sum_{\substack{m=0 \\ m\neq k}}^{N_c-1} X_m H_m^{(i)} \Lambda_{k-m}^{(i)}}_{\text{ICI term}} + V_k^{(i)} \qquad \forall i = 1,2 \tag{4.10}$$

where X_k and $H_k^{(i)}$ are the Fourier transform of x_n and $h_n^{(i)}$, respectively. The values $\Lambda_0^{(i)}$ and $\Lambda_{k-m}^{(i)}$ for $m \neq k$ in the first and second terms in (4.10) denote CPE and ICI, respectively. Finally $V_k^{(i)}$ is the noise in the frequency domain. The output of MRC is given by

$$\tilde{Y}_{k,MRC} = \left[\Lambda_0^{(1)} H_k^{(1)}\right]^* Y_k^{(1)} + \left[\Lambda_0^{(2)} H_k^{(2)}\right]^* Y_k^{(2)} \tag{4.11}$$

Thus, we can calculate mean and variance of $\tilde{Y}_{k,MRC}$ as follows

$$\begin{aligned} \mu_{\tilde{Y}_{k,MRC}} &= a_{k,MRC} X_k \\ \sigma^2_{\tilde{Y}_{k,MRC}} &= \frac{1}{N_c{}^2} \sum_{i=1}^{2} \sum_{m=0,m\neq k}^{N_c-1} \left[\underbrace{\Lambda_0^{(i)*} \Lambda_{k-m}^{(i)} H_k^{(i)*} H_m^{(i)}}_{\text{ICI}} \right] + N_c a_{k,MRC} \sigma_V^2 \end{aligned} \tag{4.12}$$

where $a_{k,MRC} = \frac{1}{N_c}\left[\left|\Lambda_0^{(1)} H_k^{(1)}\right|^2 + \left|\Lambda_0^{(2)} H_k^{(2)}\right|^2\right]$. Finally, BER for MRC can be obtained by

$$P_{e,MRC} = \frac{1}{N_c}\sum_{k=0}^{N_c-1} Q\left(\frac{a_{k,MRC}}{\sigma_{U_{k,MRC}}}\right) = \frac{1}{N_c}\sum_{k=0}^{N_c-1} Q\left(\frac{1}{\sqrt{\frac{\text{ICI term}}{N_c{}^2 a_{k,MRC}^2} + \frac{\sigma_V^2}{N_c a_{k,MRC}}}}\right) \quad (4.13)$$

From (4.13), it shows that diversity gain gives a direct solution for joint suppression of ICI and noise.

4.3.2 ICI Compensation Using Lowpass Filtering in Transfer Domain

Since the variation of the channels is substantially slower than those of ICI and noise, the transformation scheme such as DFT/FFT can be used for filtering both ICI and noise [33]. That is, after passing through extra DFT/FFT, ICI or noise effects in high frequency can be removed by a lowpass filter. One such approach has been discussed in Section 3.4.2.

4.3.3 Decision Feedback Phase Noise Compensator

As mentioned in Section 3.4, the LS-based channel estimation incorporating linear interpolation is simple to implement. However, it induces several disadvantages. As ICI and noise exist, the correct channel estimates at the pilot locations are hard to be achieved. In addition, since ICI and/or noise effects change randomly, the linear interpolation cannot distortionlessly obtain the channel estimates, and the receiver then fails to successfully restore the transmitted data. In order to alleviate the ICI effects generated by phase noise, we propose a decision feedback algorithm with batch processing, as shown in Fig. 4.14, for phase noise compensation [34]. The design of the receiver involves the following procedure. First, conventional LS-based channel estimation with linear interpolation is applied on the pilot tones to obtain the preliminary channel estimates. MRC along with the estimated channel is then performed on the received signal to decode the transmitted data. Finally, the corresponding result is sent back to an MMSE processor to further enhance the system performance. Mathematically speaking, the optimal weights of an MMSE processor can be obtained by minimizing the cost function given by

$$\mathbf{W}_d = \arg\min_{\mathbf{W}_d} \mathrm{E}\left\{\left|\mathbf{W}_d^H \mathbf{Y}_d - \hat{X}_d\right|^2\right\} \tag{4.14}$$

whose solution is

$$\mathbf{W}_d = \mathbf{R}_y^{-1}\mathbf{r}_{yd} \tag{4.15}$$

where $\mathbf{Y}_d$ and $\hat{X}_d$ denote the received data and the preliminarily estimated data in the frequency domain, respectively, and

$$\begin{aligned}
\mathbf{R}_y &= \mathrm{E}\left\{\mathbf{Y}_d \mathbf{Y}_d^H\right\} \approx \frac{1}{N_b}\sum_{n=1}^{N_b} \mathbf{Y}_d(n)\mathbf{Y}_d^H(n) = \frac{1}{N_b}\sum_{n=1}^{N_b}\begin{bmatrix} Y_d^{(1)}(n) \\ Y_d^{(2)}(n)\end{bmatrix}\begin{bmatrix} Y_d^{(1)}(n) \\ Y_d^{(2)}(n)\end{bmatrix}^H \\
\mathbf{r}_{yd} &= \mathrm{E}\left\{\mathbf{Y}_d \widehat{X}_d^*\right\} \approx \frac{1}{N_b}\sum_{n=1}^{N_b} \mathbf{Y}_d(n)\widehat{X}_d^*(n) = \frac{1}{N_b}\sum_{n=1}^{N_b}\begin{bmatrix} Y_d^{(1)}(n) \\ Y_d^{(2)}(n)\end{bmatrix}\widehat{X}_d^*(n),
\end{aligned} \tag{4.16}$$

where N_b is the sample size in the time domain and $Y_d^{(i)}(b) = H_d^{(i)} X_d^{(i)}(b) + N_d^{(i)}(b)$ is the received signal, with *d*, *i*, and *b* being data tone, the *i*th antenna, and the *b*th OFDM symbol, respectively. In the following, we will examine the corresponding advantages and limitations of this scheme under different situations.

It is noteworthy that the noise term in (4.16) can be further suppressed by using a summation operator for processing more data simultaneously. In many decision-feedback systems, the error propagation problem is a critical issue. We assume that the preliminarily estimated data is sufficiently reliable, i.e. BER is smaller than 0.1. The decoded data with errors spreads in the cross-correlation $\mathbf{r}_{yd}$. Similarly, the error term dies away by summing more symbols. Therefore, the summation function plays a role of ICI, noise, and error suppression. In addition, we concentrate on the $\mathbf{R}_y$ in (4.16). We need to, by some means or other, calculate signals respectively in different branches, i.e.

$$\begin{aligned}
R_y^{(i)'} &= \mathrm{E}\left\{Y_d^{(i)} Y_d^{(i)*}\right\} \approx \frac{1}{N_b}\sum_{n=1}^{N_b} Y_d^{(i)}(n) Y_d^{(i)*}(n) \qquad i = 1, 2 \\
r_{yd}^{(i)} &= \mathrm{E}\left\{Y_d^{(i)} \widehat{X}_d *\right\} \approx \frac{1}{N_b}\sum_{n=1}^{N_b} Y_d^{(i)}(n)\widehat{X}_d^*(n)
\end{aligned} \tag{4.17}$$

This implies that in (4.17), auto- and cross-correlations are computed in different branches separately, while they are obtained in different branches jointly in (4.16). In each batch processing, solving (4.15) needs twelve multipliers and one divider with

(4.16), but needs six multipliers and two dividers with (4.17). We know that gate counts of divider are larger than those of multiplier, i.e. the former needs lower computational complexity than that of the latter. Moreover, we use MRC to enhance decision accuracy and improve system performance. Furthermore, since the iterative procedure is processed based on the Viterbi output, the scheme passes through inner deinterleaver and Viterbi blocks twice. Thus, with feedback scheme used, coding gain can be increased. The decision feedback phase noise compensation scheme with batch processing possesses advantages as mentioned above such that the improved DVB-T system can enhance the robustness against ICI and larger phase noise variance.

4.3.4 Batch Processing in Time-Frequency Domain

As mentioned above, with batch processing in the time domain used, more data samples can be used to alleviate ICI or phase noise. The system performance is dependent on the sample size. The channel response may vary for larger processing period, i.e. larger sample size, and then the system performance will degrade, while with smaller sample size selected, the effects of ICI and phase noise fails be improved due to the lack of enough processed data. Hence, the determination of the sample size will be a trade-off problem between channel variation and ICI compensation. With the proper sample size used, batch processing in the time domain can effectively alleviate the ICI and phase noise effects. However, over the fast fading channel introduced by the high speed vehicle or the environmental components, this method fails to successfully suppress ICI and noise and retain the desired signals during the processing period, leading to substantially degradation in performance. As a remedy, batch processing in the frequency domain can be used when the coherence bandwidth is sufficiently large. Unfortunately, this method cannot effectively combat the ICI and phase noise effects in the case of smaller coherent bandwidth. Hence, we propose a novel batch processing technique in the time-frequency domain to achieve a good trade-off between channel variation and phase noise compensation with proper sample sizes used in both dimensions. The corresponding schematic diagrams of the phase noise compensators incorporating batch processing in the time, frequency, and time frequency dimensions are shown in Figs. 4.15-17.

4.3.5 Determination of Sample Size

In the following, according to the theoretical analysis, we will discuss the determination of sample size in the case of the batch processing technique for ICI and noise compensation applied in both the time- and frequency-domains. The RMS delay spread of a Rayleigh fading channel in a DVB-T system is given by

$$\tau_{rms} = \frac{\sum_k \alpha_k^2 \tau_k}{\sum_k \alpha_k^2} \approx 1.2689 \quad (\mu s) \tag{4.18}$$

where α_k and τ_k denote the complex amplitude and the delay associated with the *k*th finger. The corresponding coherence bandwidth is given by

$$B_c \approx \frac{1}{5\tau_{rms}} = 157.62 \quad \text{(KHz)} \tag{4.19}$$

The tone spacing in a DVB-T system of 8 MHz bandwidth is 3.9625 KHz such that there are about 40 tones within the coherence bandwidth. When the batch processing scheme is used in the frequency domain, the optimal sample size is obtained based on the coherence bandwidth in (4.19). In addition, the coherence time will be derived in terms of velocity (Doppler frequency). The Doppler frequency for a moving terminal with velocity *v* is given by

$$f_d \approx v \frac{f_{UHF}}{c} \tag{4.20}$$

where f_{UHF} and *c* are the carrier frequency in UHF band and light speed, respectively. The coherence time can be expressed as

$$T_c \approx \frac{9}{16\pi f_d} \tag{4.21}$$

When we exploit batch processing in the time domain, the optimal sample size can be chosen based on the coherence time in (4.21). Suppose the velocity is 5 m/s for example. The corresponding Doppler frequency f_d is about 7.9 Hz such that the coherence time is about 22700 μs. Since the duration of an OFDM symbol in DVB-T systems is 280 μs, there are about 81 OFDM symbols within the coherence time.

4.4 Computer Simulations

In this section, computer simulations are conducted to evaluate the BER performance of DVB-T systems. Throughout the simulations, we only deal with the discrete time signal processing of the baseband; hence pulse-shaping and matched-filtering are removed for simplicity. In addition, timing synchronization is assumed to be perfect. All channel parameters are listed in Table 3.6. Unless otherwise mentioned, the following parameters are assumed: phase noise variance = 0.1 and mobile velocity v = 5 m/s. In the first simulation, the efficacy of the phase noise compensation scheme using batch processing in the time domain is evaluated with the sample size varied. The BER performances as a function of input SNR E_b/N_0 shown in Figs. 4.18(a)-(c) for phase noise variance = 0.4, 0.1, and 0.04, respectively, indicate that the system performances are degraded as the phase noise variance increases. It is observed that the algorithm with too smaller or larger sample size leads to worse performance. This is because that the smaller sample size cannot completely compensate the phase noise effect due to lack of enough sampled data. On the other hand, in the case of larger sample size, the variation of channel will destroy the assumption of fixed channel condition during the processing time and then fail to successfully collect the desired signals, leading to performance degradation. It is noteworthy that in this simulation, the optimal performance can be achieved by the optimal sample size N_b equaling to 34.

In the second simulation, the efficacy of the phase noise compensation scheme with batch processing in the frequency domain is examined with the sample size varied. The BER performances shown in Figs. 4.19(a)-(c) corresponding to Figs. 4.18(a)-(c), respectively, follow the same trend as observed in the time domain processing, except that the optimal sample size N_b equals to 24 which is smaller than that obtained in Fig. 4.18. In addition, the frequency domain processing exhibits significant performance degradation as compared to the time domain method. This is because sample size within the coherence time is larger than that within the coherence bandwidth as long as channel variation is not obvious.

In the third simulation, the efficacy of the phase noise compensation scheme with batch processing in the time-frequency domain is investigated with the sample size

varied. The BER performances shown in Figs. 4.20 for the phase noise variance = 0.1 follow the same trend as observed in Fig. 4.18(b), except that the time-frequency domain processing outperforms both the time and frequency domain processing.

In the fourth simulation, the fading effect on the phase noise compensation schemes with batch processing in the time domain is investigated with mobile velocity v = 20 m/s and the sample size varied. The result shown in Fig. 4.21 indicates that the performance is worse than that of mobile velocity v = 5 m/s in Fig. 4.18 due to the severe fading. Furthermore, the optimal sample size of $N_b = 16$ is smaller than that obtained in Fig. 4.18(b), which is $N_b = 34$. This is because channel response may change severely in time dimension when the mobile velocity is fast; hence larger sample size will significant degrade the system performance.

In the final simulation, a comparison among the conventional MRC, and the phase noise compensation schemes with batch processing in the time, frequency, and time-frequency domains is investigated with the sample size varied. In this simulation, the optimal sample sizes $N_b = 34, 24$ and $(8,16)$ are used for batch processing in the time, frequency, and time-frequency domain, respectively. The BER performances shown in Fig. 4.22 indicate that the batch processing in the time-frequency domain outperforms the other methods. This is because channel variation in time-frequency processing is much slower, leading to successful suppression of phase noise and significant performance enhancement.

4.5 Summary

In this chapter, we first review the diversity reception schemes including MRC, SBSD, CDD, MRC with CDD, IVSD, PVSD, and PBSD. The corresponding performance and computational complexity are then investigated. Among them, the selection between the selective and combining diversity schemes is based on the trade-off between BER performance and computational complexity. In addition, in order to improve the performance degradation due to phase noise, we propose the decision feedback phase noise compensation scheme incorporating batch processing in the time, frequency, or time-frequency domain. The proposed receiver is shown to outperform the conventional MRC method and enhance robustness against phase noise.

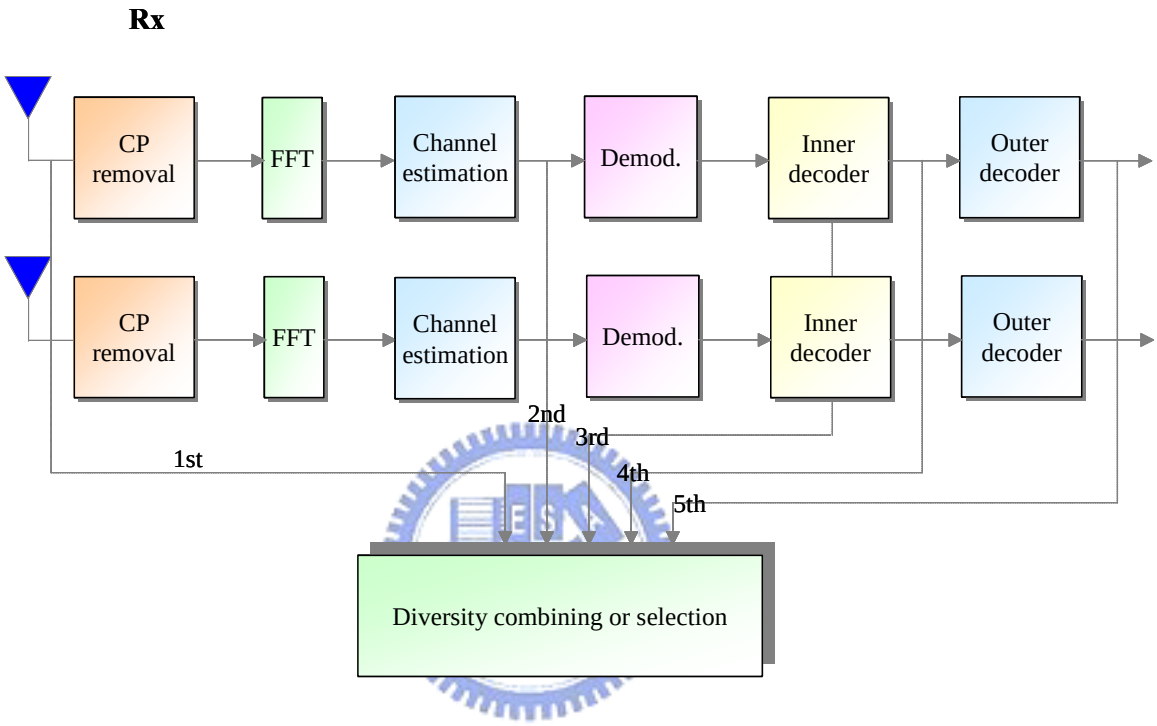

Figure 4.1: Various diversity reception schemes at different stages in DVB-T system.

1st stage: symbol-based selective diversity (SBSD) and cyclic delay diversity (CDD).
2nd stage: MRC and MRC with CDD.
3rd stage: in-Viterbi selective diversity (IVSD).
4th stage: post-Viterbi selective diversity (PVSD).
5th stage: packet-based selective diversity (PBSD).

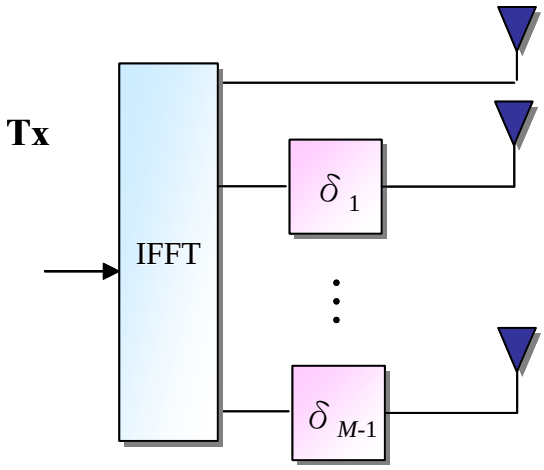

Figure 4.2: OFDM system with delay diversity at transmitter side.

(a) (b)

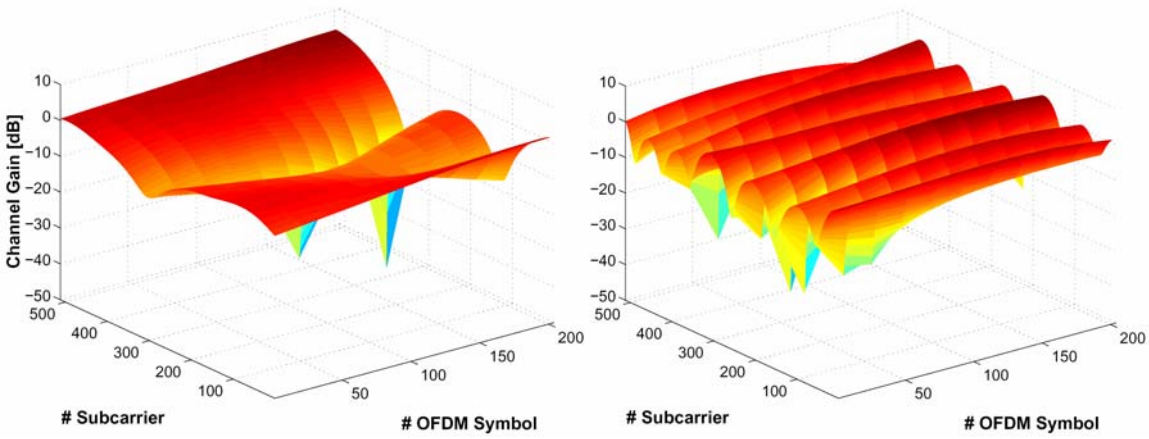

Figure 4.3: Effect of DD over a typical indoor channel. (a) Without DD. (b) With DD.

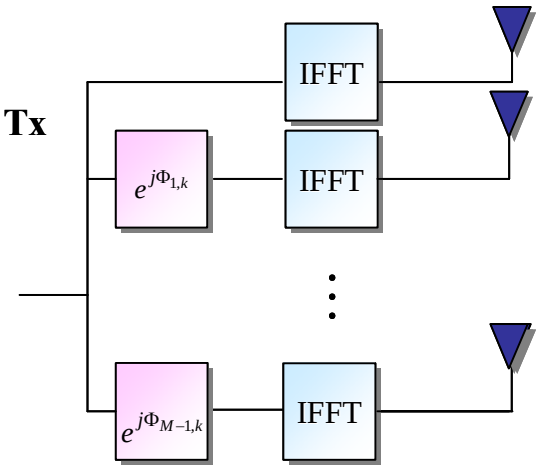

Figure 4.4: OFDM system with phase diversity at transmitter side.

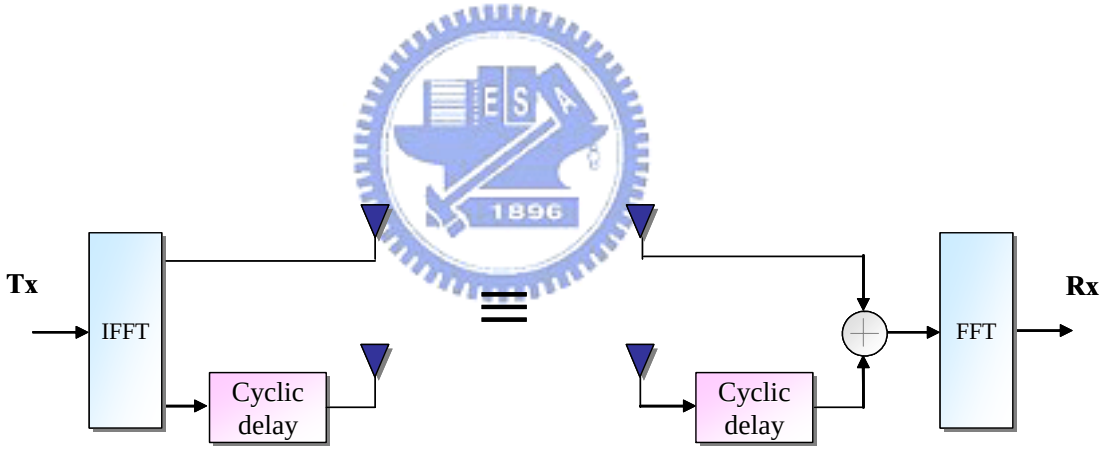

Figure 4.5: Equivalent model of transmitter and the receiver with CDD in OFDM system.

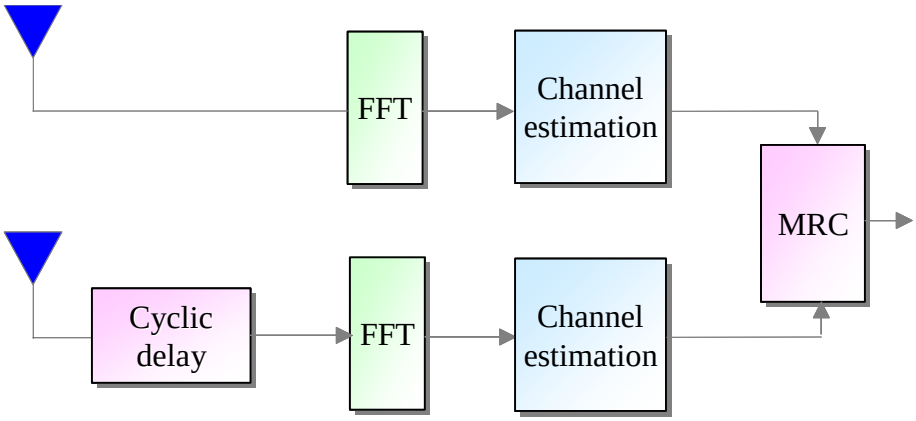

Figure 4.6: MRC with CDD at receiver side in OFDM system.

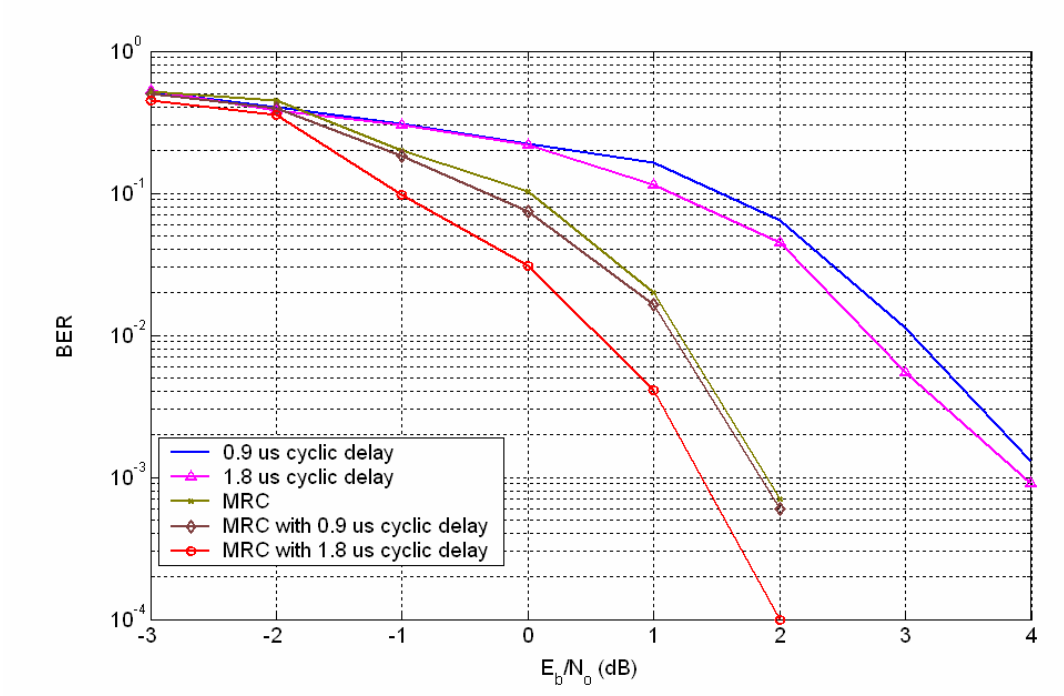

Figure 4.7: BER performances of CDD and MRC in DVB-T systems with cyclic delay varied as a parameter.

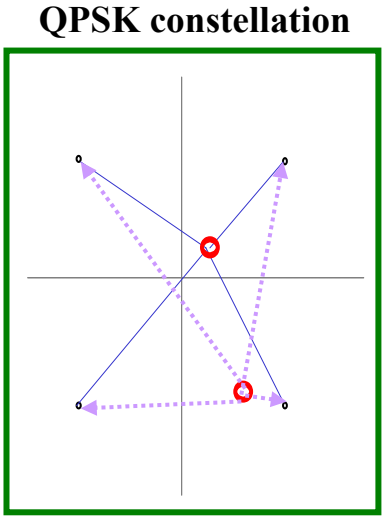

Figure 4.8: Illustration of symbol location induced by random noise under QPSK constellation.

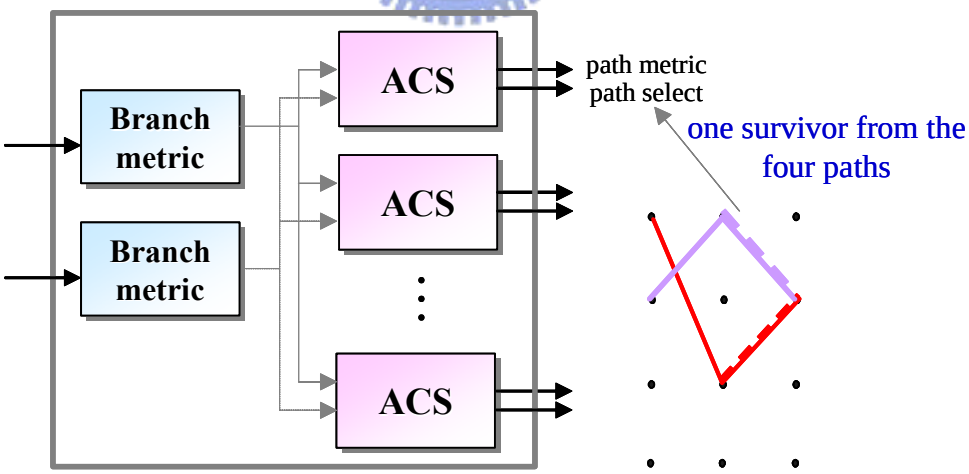

Figure 4.9: Illustration of diversity reception scheme with IVSD.

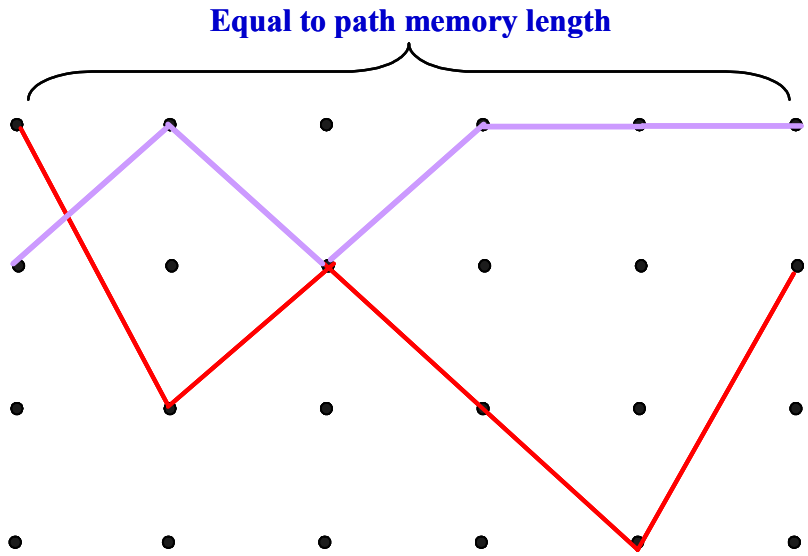

Figure 4.10: Different branches selected and compared after passing through a long path after Viterbi decoding.

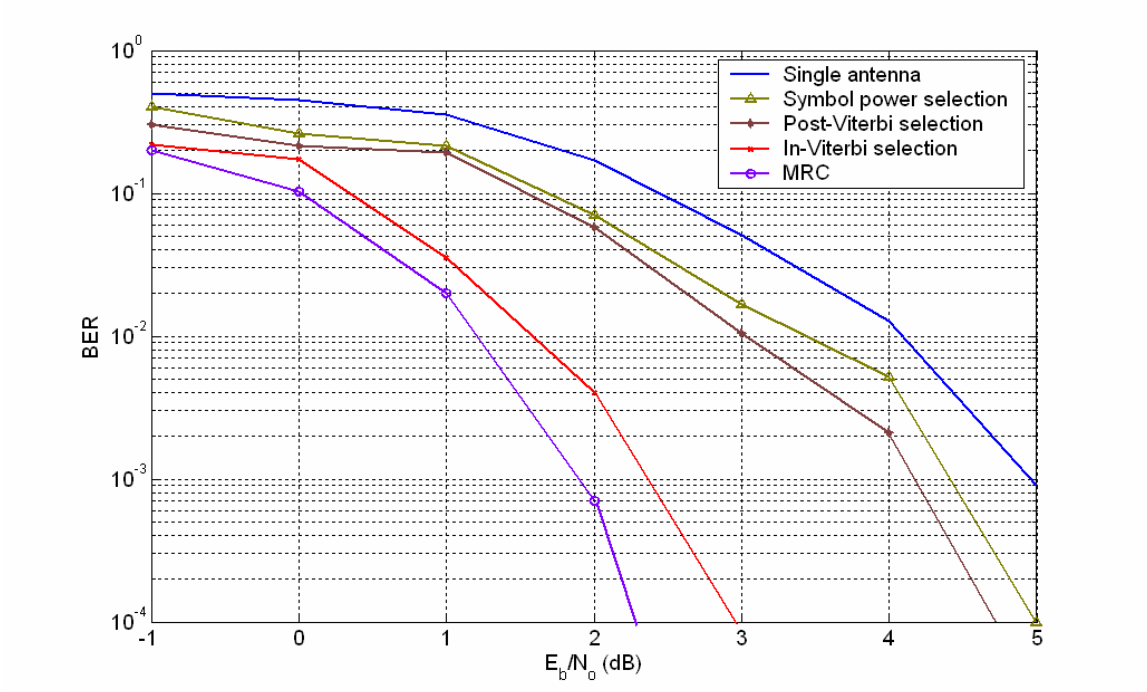

Figure 4.11: BER performances of different diversity reception schemes in DVB-T system.

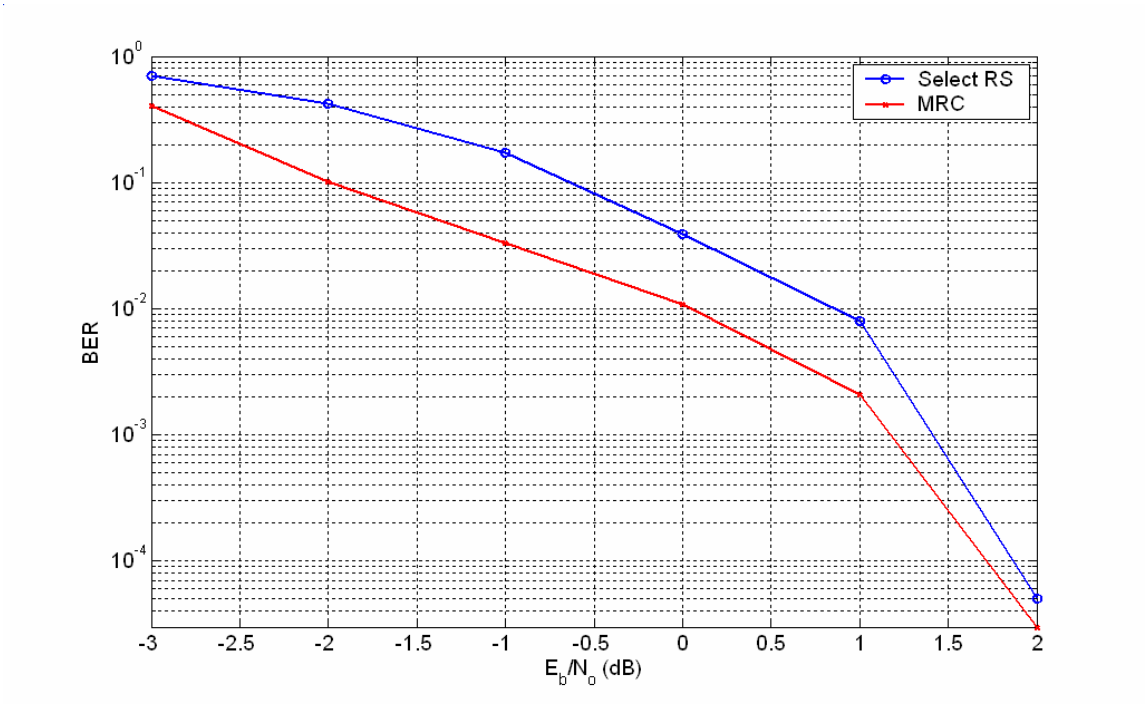

Figure 4.12: BER performance of MRC and PBSD decoder with outer channel coding in DVB-T system.

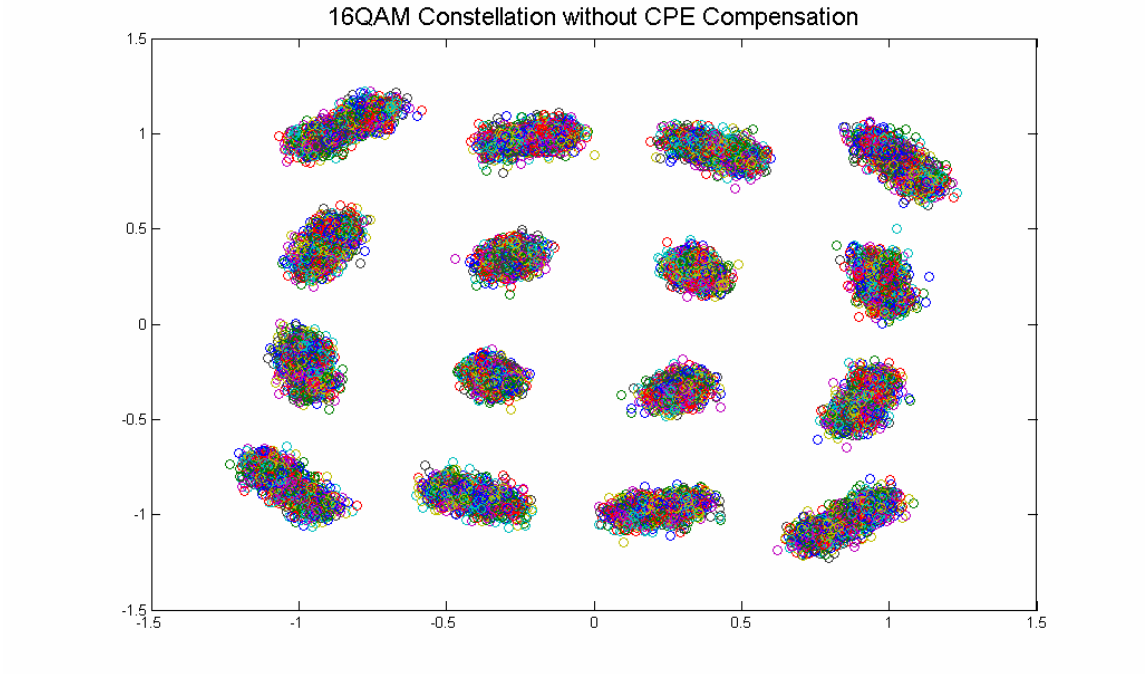

Figure 4.13: 16QAM signals without compensating CPE effect induced by phase noise in frequency domain.

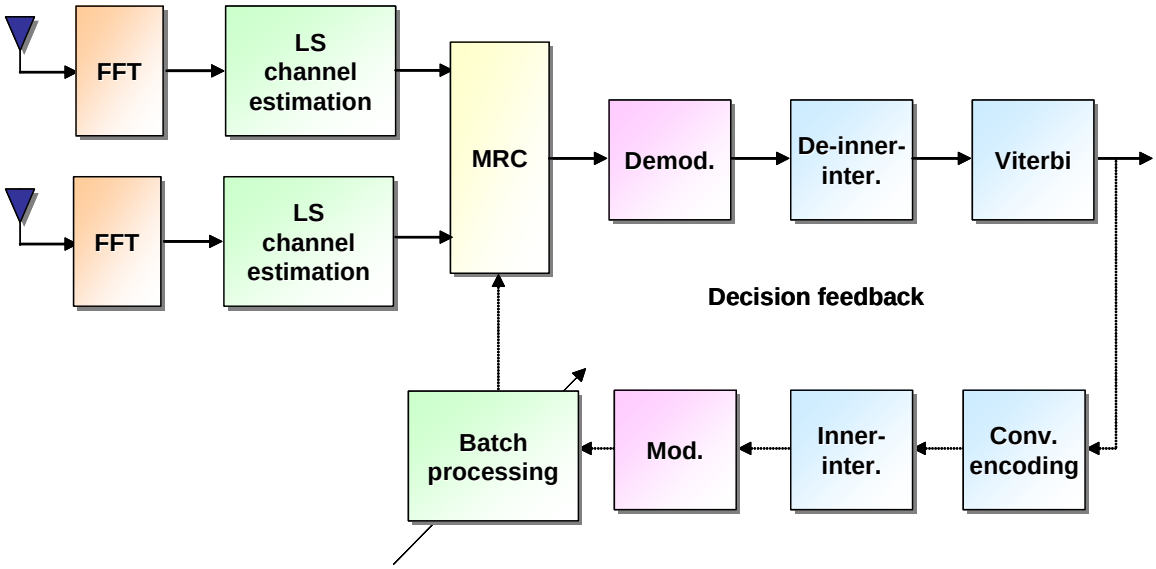

Figure 4.14: Illustration of decision feedback phase noise compensator with batch processing in DVB-T system.

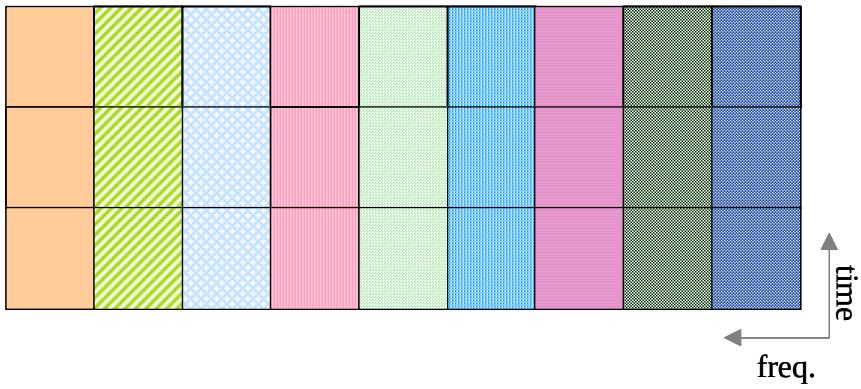

Figure 4.15: Phase noise compensation using batch processing for collection of OFDM symbols in time domain.

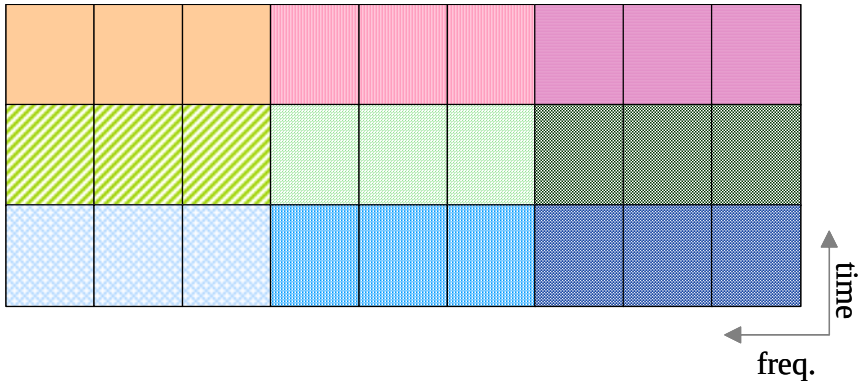

Figure 4.16: Phase noise compensation using batch processing for collection of data tones in frequency domain.

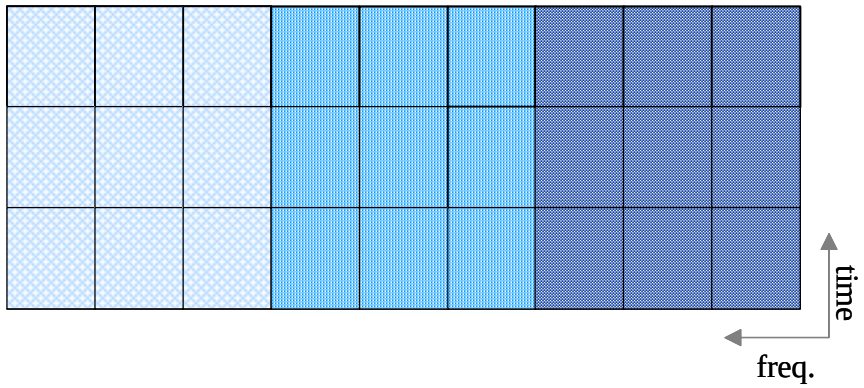

Figure 4.17: Phase noise compensation using batch processing for collection of OFDM symbols and data tones in time-frequency domain.

(a)

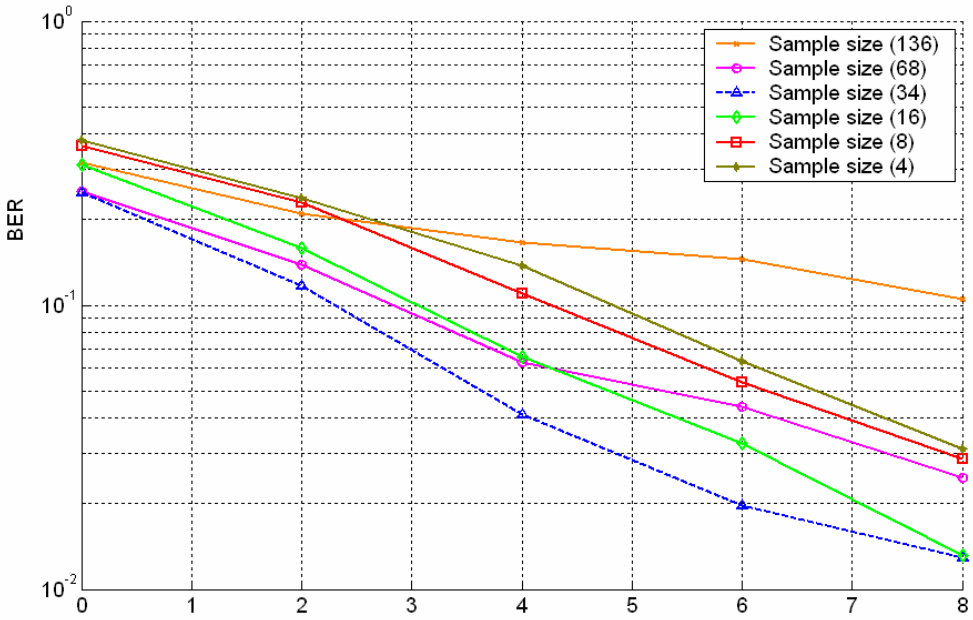
BER
Sample size (136)
Sample size (68)
Sample size (34)
Sample size (16)
Sample size (8)
Sample size (4)

(b)

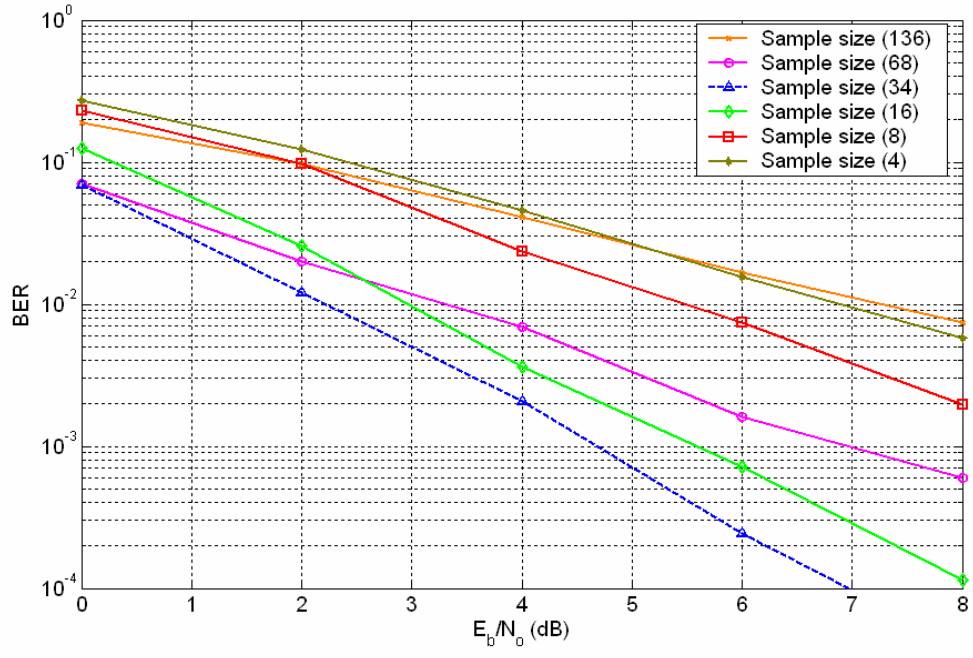
BER
Sample size (136)
Sample size (68)
Sample size (34)
Sample size (16)
Sample size (8)
Sample size (4)
Eb/No (dB)

(c)

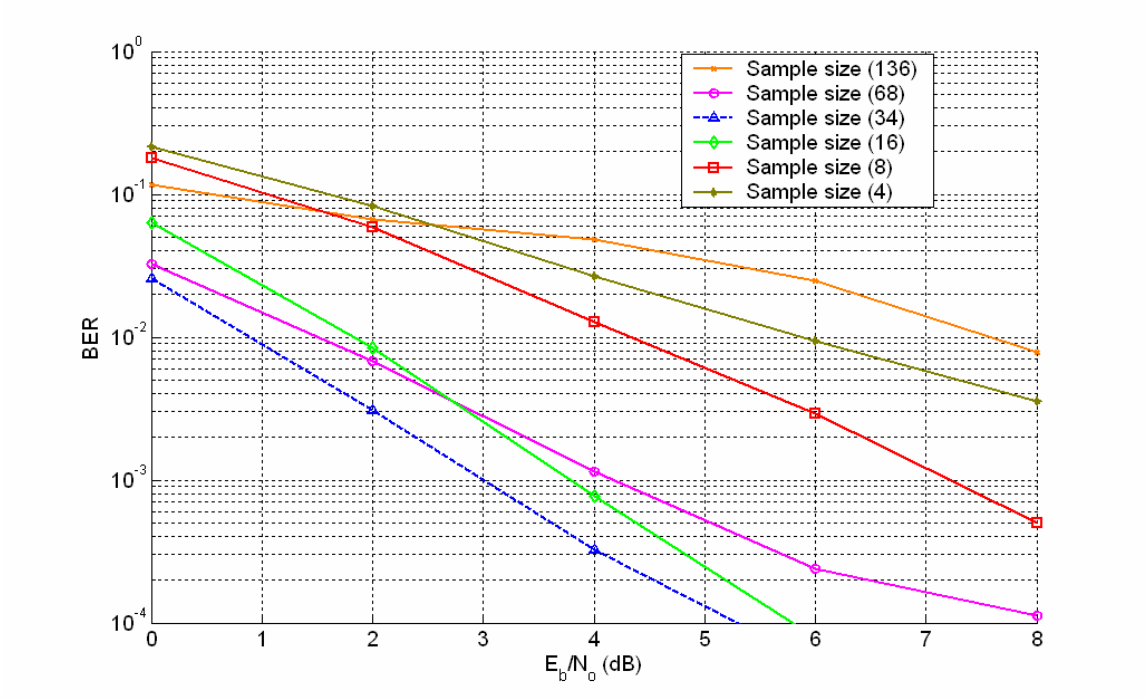

Figure 4.18: BER performances obtained by using phase noise compensation in time domain with sample size varied and velocity v = 5 m/s. (a) Phase noise variance = 0.4. (b) Phase noise variance = 0.1. (c) Phase noise variance = 0.04.

(a)

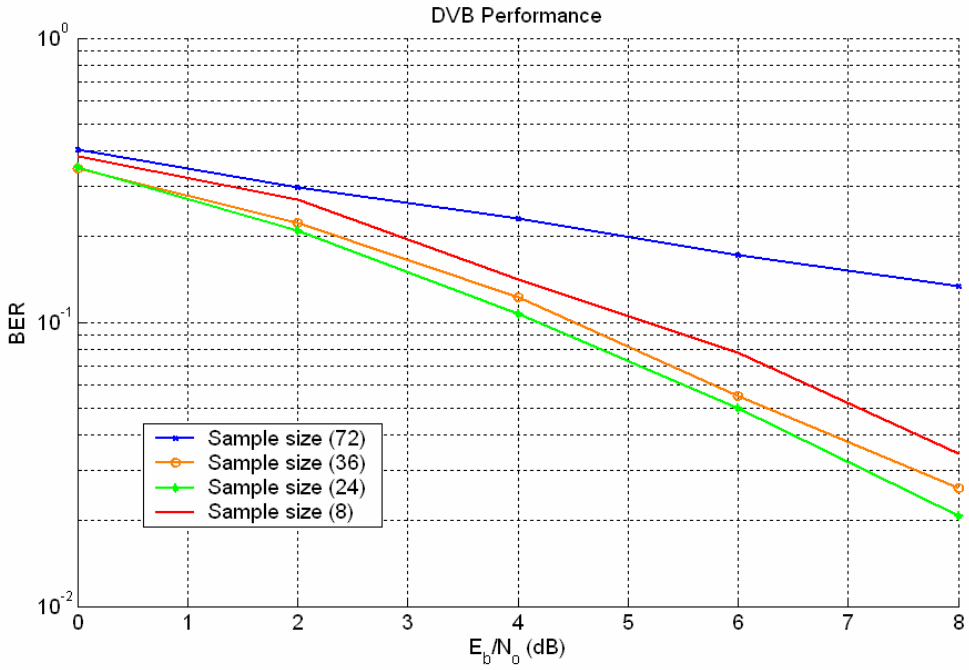
DVB Performance
BER
10^0
10^{-1}
10^{-2}
0
1
2
3
4
5
6
7
8
E_b/N_o (dB)
Sample size (72)
Sample size (36)
Sample size (24)
Sample size (8)

(b)

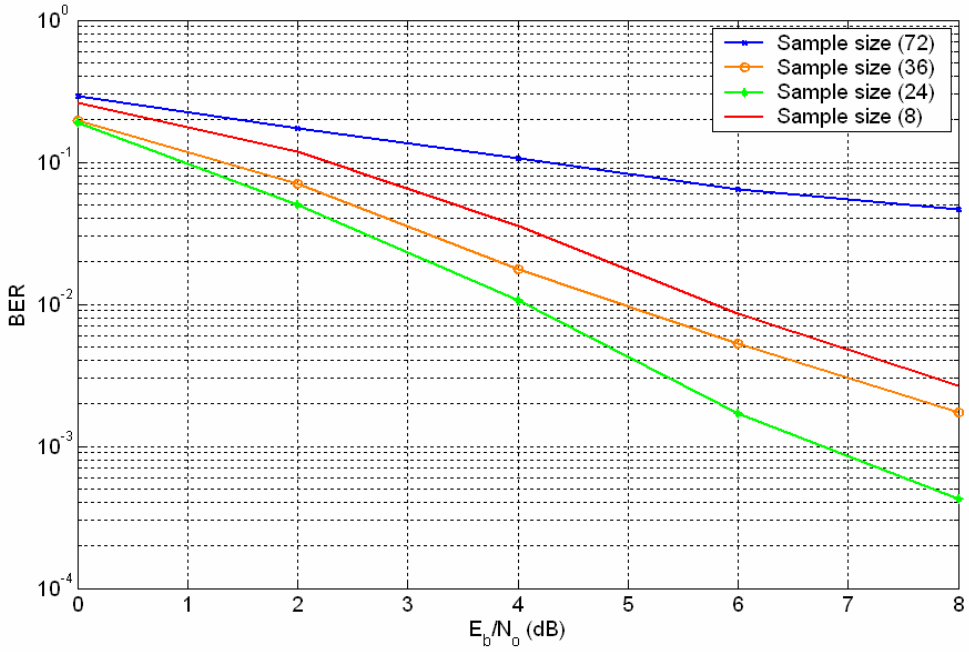
BER
10^0
10^{-1}
10^{-2}
10^{-3}
10^{-4}
0
1
2
3
4
5
6
7
8
E_b/N_o (dB)
Sample size (72)
Sample size (36)
Sample size (24)
Sample size (8)

(c)

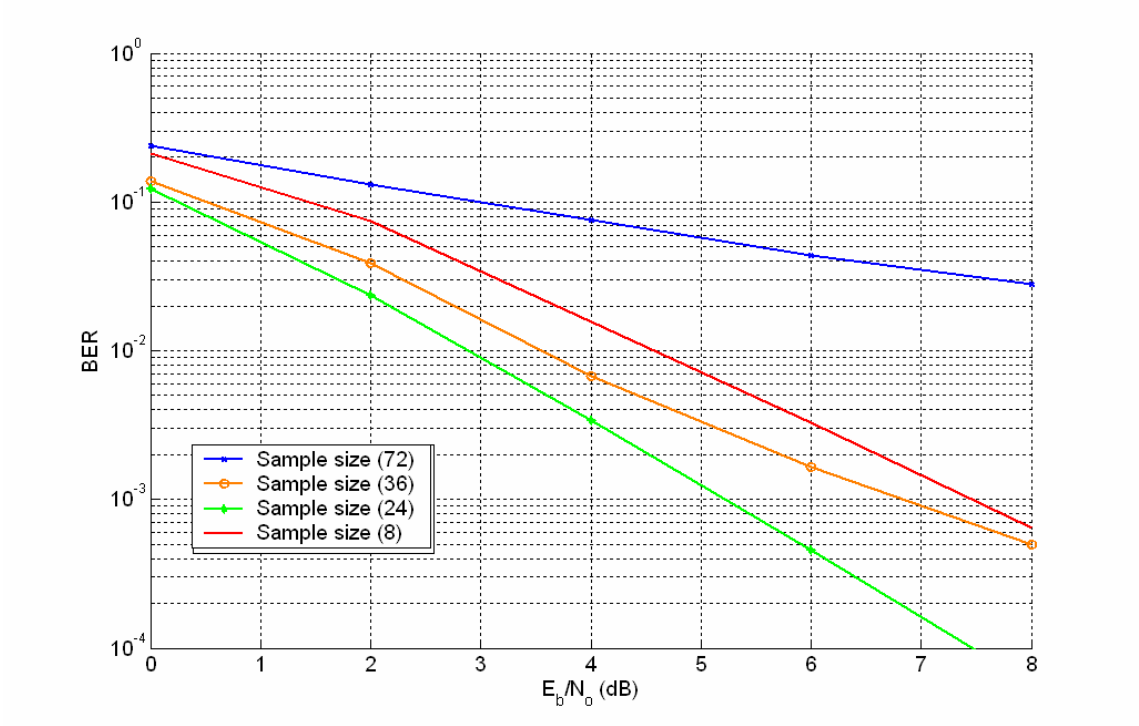

Figure 4.19: BER performances obtained by using phase noise compensation in frequency domain with sample size varied and velocity v = 5 m/s. (a) Phase noise variance = 0.4. (b) Phase noise variance = 0.1. (c) Phase noise variance = 0.04.

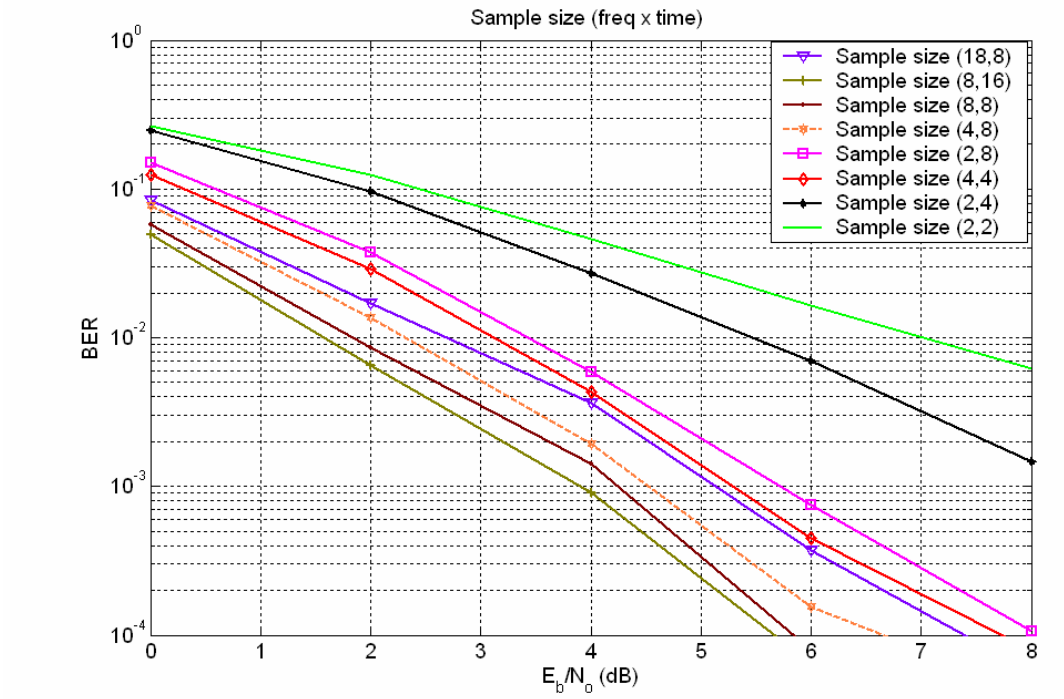

Figure 4.20: BER performances obtained by using phase noise compensation in time-frequency domain with sample size varied, velocity v = 5 m/s and phase noise variance = 0.1.

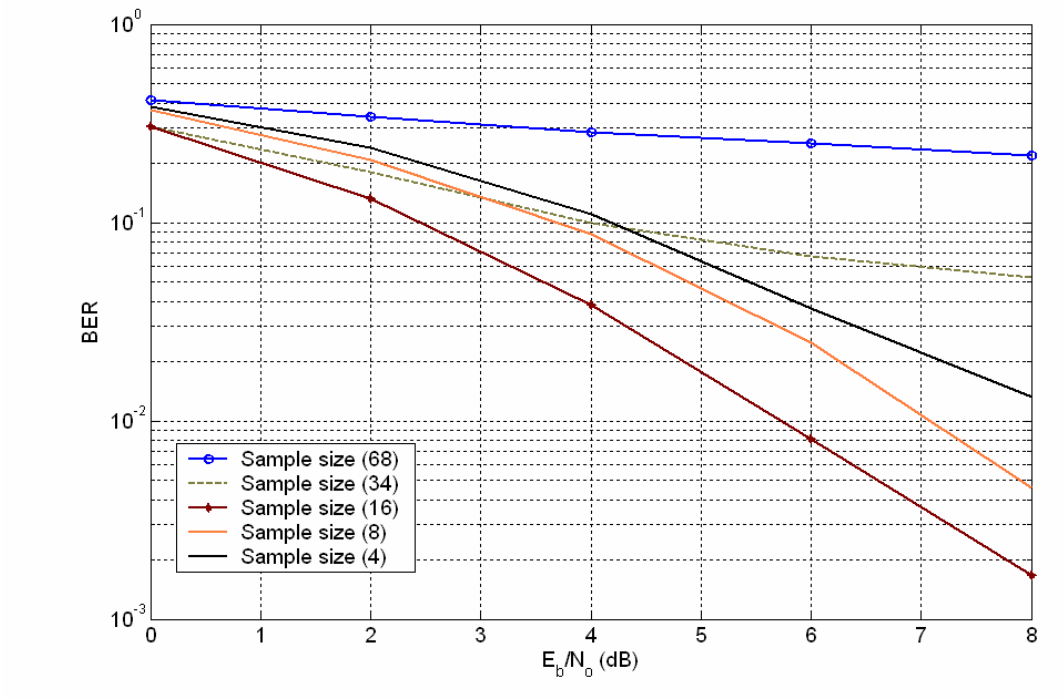

Figure 4.21: BER performances obtained by using phase noise compensation in time domain with sample size varied, velocity v = 20 m/s and phase noise variance = 0.1.

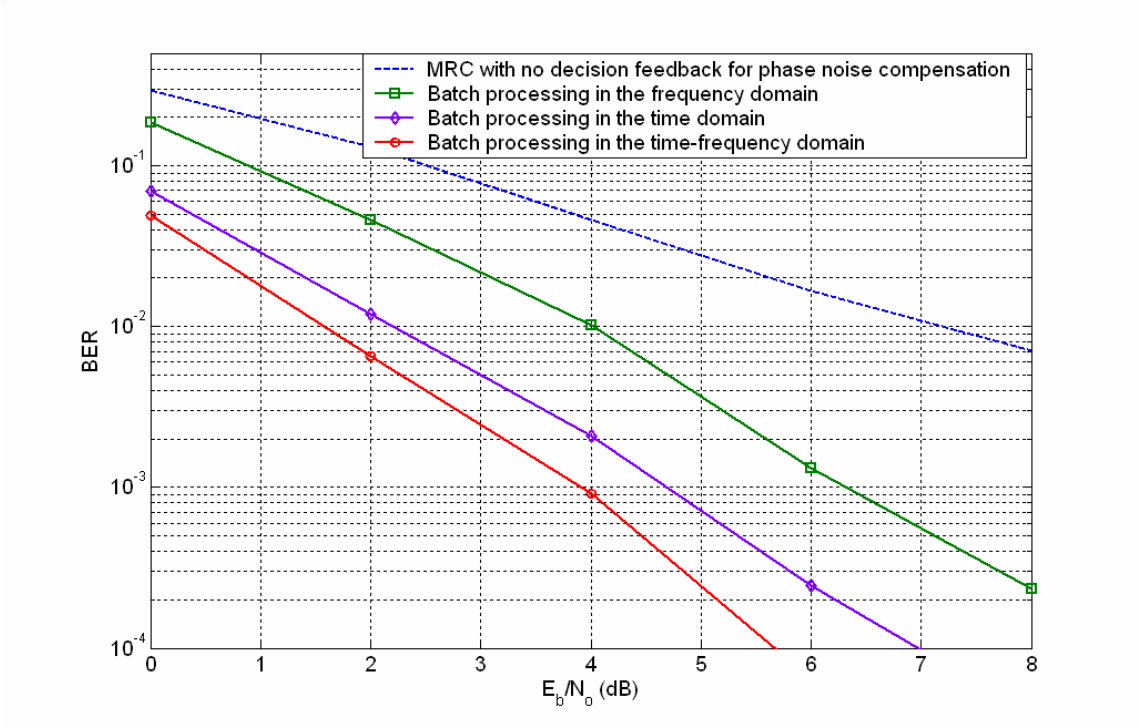

Figure 4.22: BER performances obtained by using conditional MRC and phase noise compensation in time, frequency, and time-frequency domain with velocity v = 5 m/s and phase noise variance = 0.1.

Chapter 5

Conclusion

In this thesis, we propose a DVB-T system incorporating diversity reception and phase noise compensation schemes. With the aid of diversity reception algorithms, we show that the receiver can achieve better link performance and provide robustness against fading effects due to multipath. On the other hand, the phase noise compensator can successfully combat the phase noise introduced by the imperfect oscillators at the transmitter and receiver sides. In Chapter 2, some key concepts of the receive diversity techniques have been introduced; the effects of phase noise and Doppler shift in an OFDM system are also studied. Furthermore, with diversity scheme used, a receiver with enhanced system performance is presented for suppression of phase noise and ICI.

In Chapter 3, based on the DVB-T technical specification, we construct a simulation platform of a DVB system using Matlab and ADS software tools used. Synchronization and channel estimation algorithms for a DVB-T receiver are also investigated. In particular, we present two feasible synchronization schemes: One is cyclic-prefix-based synchronization, which enables self-synchronization in an OFDM system. Self-synchronization is an idea to exploit the duplication characteristic of cyclic prefix in OFDM symbols. The other one is pilot-based synchronization using a pilot-correlation detector to extract the synchronization information at the pilot tones from the received signal. With regards to channel estimation, the LS channel estimation with linear interpolation and the lowpass filtering in the transform domain are included for refining estimation of the channel response, in which the LS-based channel estimation is aimed to be implemented with lower complexity while the other is

targeted at better performance.

In Chapter 4, the diversity reception and phase noise compensation algorithms are presented. We first review the diversity reception schemes including MRC, SBSD, CDD, MRC with CDD, IVSD, PVSD, and PBSD. The corresponding performance and computational complexity are then investigated. Among them, the selection between the selective and combining diversity schemes is based on the trade-off between BER performance and computational complexity. In order to combat phase noise, we propose the decision feedback phase noise compensation scheme incorporating batch processing in the time, frequency, or time-frequency domain. It is shown that the proposed scheme outperforms the conventional MRC method and enhances robustness against phase noise.

The study presented in the thesis has thoroughly discussed the receiver design for a DVB-T system and its efficacy has been rigorously verified using the simulation platform. In particular, we deliver feasible solutions to advanced DTV systems. In practice, there are yet several other limitations remaining to be considered in implementing a DVB-T system, such as memory usage, operating speed, and gate counts. For the sake of fast development and low cost, the development platform should adopt a programmable prototyping communication system including the existing functions presented in the thesis. Furthermore, a similar specification, referred to as DVB-handheld (DVB-H), is regarded as an extension to DVB-T standard. DVB-H is envisioned as a "one-to-many" broadcast project, enabling the distribution of music, film clips or other multimedia contents to a large audience via mobile handsets. A critical issue in DVB-H is power consumption. In conclusion, developing a compliant hardware platform for DVB-T and detailed algorithms for DVB-H will be a challenge in the future.

Bibliography

[1] J. Rinne, “Some elementary suboptimal diversity reception schemes for DVB-T in mobile conditions,” *Consumer Electronics, IEEE Transactions on*, Vol. 46, No. 3, pp. 847-850, Aug. 2000.

[2] S. Kaiser, “Spatial transmit diversity techniques for broadband OFDM systems,” *GLOBECOM '00, IEEE*, Vol. 3, pp. 1824-1828, Nov.-Dec. 2000.

[3] K. Witrisal, Y. H. Kim, R. Prasad, and L. P. Ligthart, “Antenna diversity for OFDM using cyclic delays,” *SCVT’01, Benelu*, pp. 13-17, Oct. 2001.

[4] M. Bossert, A. Huebner, F. Schuehlein H. Haas, and E. Costa, “On cyclic delay diversity in OFDM based transmission schemes,” *InOWo’02, Hamburg*, 5 pages on CD-Rom, Sep. 2002.

[5] A. Dammann and S. Kaiser, “Standard conformable antenna diversity techniques for OFDM and its application to the DVB-T system,” *GLOBECOM '01, IEEE*, Vol. 5, pp. 3100-3105, Nov. 2001.

[6] T. Sakai, K. Kobayashi, S. Kubota, M. Morikura, and S. Kato, “Soft-decision Viterbi decoding with diversity combining,” *GLOBECOM '90. IEEE*, Vol. 2, pp. 1127-1131, Dec. 1990.

[7] T. Sakai, K. Kobayashi, S. Kubota, M. Morikura, and S. Kato, “Soft-decision Viterbi decoding with diversity combining for multi-beam mobile satellite communication systems,” *Selected Areas in Communications, IEEE Journal on*, Vol. 13, No. 2, pp. 285-290, Feb. 1995.

[8] T. Onizawa, M. Mizoguchi, T. Sakata, and M. Morikura **“**A new simple adaptive phase tracking scheme employing phase noise estimation for OFDM signals,” *VTC’02, IEEE*, Vol. 3, pp. 1252-1256, May 2002.

[9] L. Piazzo, and P. Mandarini **“**Analysis of phase noise effects in OFDM modems,” *Communications, IEEE Transactions on*, Vol. 50, No. 10, pp. 1696-1705, Oct. 2002.

[10] H. G.. Ryu, and Y. S. Lee **“**Phase noise analysis of the OFDM communication system by the standard frequency deviation,” *Consumer Electronics, IEEE Transactions on*, Vol. 49, No. 1, pp. 41-47, Feb. 2003.

[11] V. Simon, A. Senst, M. Speth, and H. Meyr **“**Phase noise estimation via adapted interpolation,” *GLOBECOM '01. IEEE*, Vol. 6, pp. 3297-3301, Nov. 2001.

[12] B. Stantchev and G. Fettweis **“**Time-variant distortions in OFDM,” *Communications, IEEE Letters on*, Vol. 4, No. 10, pp. 312-314, Oct. 2000.

[13] M. S. El-Tanany, Y. Wu, and L. Házy, “Amalytical modeling and simulation of phase noise interference in OFDM-based digital television terrestrial broadcasting systems,” *Broadcasting, IEEE Transactions on*, Vol. 47, No. 1, Mar. 2001.

[14] A. García Armada, “Understanding the effects of phase noise in orthogonal frequency division multiplexing (OFDM),” *Broadcasting, IEEE Transactions on*, Vol. 47, No. 2, pp. 153-159, Jun. 2001.

[15] P. Robertson and S. Kaiser, “Analysis of the effects of phase-noise in orthogonal frequency division multiplexing (OFDM) systems,” *ICC’95, Seattle*, Jun. 1995.

[16] K. Nikitopoulos and A. Polydoros, “Joint channel equalization and residual frequency offset and phase noise compensation in OFDM systems,” *InOWo’02, Hamburg*, Sep. 2002.

[17] K. Nikitopoulos and A. Polydoros, “Analysis of new and existing methods of reducing intercarrier inyerference due to carrier frequency offset in OFDM,” *Communications, IEEE Transactions on*, Vol. 47, No. 3, Mar. 1999.

[18] K. Nikitopoulos and A. Polydoros, “Compensation schemes for phase noise and residual frequency offset in OFDM systems,” *GLOBECOM '01. IEEE*, Vol.1, pp. 330-333, Nov. 2001.

[19] A. García Armada and M. Calvo, “Phase noise and sub-carrier spacing effects on the performance of an communication system,” *Communications, IEEE Letters on*, Vol. 2, No. 1, pp. 11-13, Jan. 1998.

[20] R. Narasimhan, “Performance of diversity schemes for OFDM systems with frequency offset, phase noise and channel estimation errors,” *ICC’02. IEEE*, Vol. 3, pp. 1551-1557, Apr.-May 2002.

[21] R. Narasimhan, “Performance of diversity schemes for OFDM systems with frequency offset, phase noise and channel estimation errors,” *Communications, IEEE Transactions on*, Vol. 50, No. 10, Oct. 2002.

[22] J. Shentu, K. Panta, and J. Armstrong, “Effects of phase noise on performance of OFDM systems using an ICI cancellation scheme” *Broadcasting, IEEE Transactions on*, Vol. 49, No. 2, Jun. 2003.

[23] ETSI, Digital video broadcasting (DVB), “*Framing structure, channel coding and modulation for digital terrestrial televisio*n,” *EN 300 744 v1.4.1*, Jan. 2001.

[24] M. Massel, “*Digital television DVB-T COFDM and ATSC 8-VSB,*” Digitaltvbooks.Com, Oct. 2000.

[25] T. S. Rappaport, “*Wireless Communications: Principles and Practice*,” Prentice Hall, 1999.

[26] Y. Zhao and S.-G. Häggman, “Sensitivity to Doppler shift and carrier frequency errors in OFDM systems – The consequences and solutions,” *VTC’96, IEEE*, Vol. 3, pp. 1564-1568, April-May 1996.

[27] R. van Nee and R. Prasad, “*OFDM for Wireless Multimedia Communications*,” Artech House, 2000.

[28] J. Terry and J. Heiskala, *”OFDM Wireless LANs: A Theoretical and Practical Guide*,” Sams, 2001.

[29] D. Liu, C. Wei, and C. Chang, “An extension of guard-interval based symbol and frequency synchronization technique for wireless OFDM transmission,” *VTC’01. IEEE*, Vol. 4, pp. 2324-2328, Oct. 2001.

[30] F. Classen and H. Meyr, “Frequency synchronization algorithms for OFDM systems suitable for communication over frequency selective fading channels,” *VTC’94, IEEE*, Vol. 3, pp. 1655-1653, Jun. 1994.

[31] M. Hsieh and C. Wei, ”A low-complexity frame synchronization and frequency offset compensation scheme for OFDM systems over fading channels,” *Vehicular Technology, IEEE Transactions on*, Vol. 48, No. 5, pp. 1596-1609, 1999.

[32] M. Hsieh and C. Wei, “Channel estimation for OFDM systems based on comb-type pilot arrangement in frequency selective fading channels,” *Consumer Electronics, IEEE Transactions on*, Vol. 44, No. 1, pp. 217-225, Feb. 1998.

[33] Y. Zhao and A. Huang, “A novel channel estimation method for OFDM mobile communication systems based on pilot signals and transform-domain processing,” *VTC’97, IEEE*, Vol. 3, pp. 2089-2093, May 1997.

[34] E. Al-Susa, “A predictor-based decision feedback channel estimation method for COFDM with high resilience to rapid time-variations,” *VTC’97, IEEE*, pp. 273-278, May 1997.